DRA

AEROSPACE REPORT NO.
ATR-81(7875)-2

Electrodynamic Studies of Upper and Lower Atmospheric Coupling

Prepared by

Y. T. CHIU, J. M. CORNWALL, B. C. EDGAR,
M. SCHULZ, and L. R. SHARP
Space Sciences Laboratory

1 March 1981

Prepared for

NATIONAL AERONAUTICS AND SPACE ADMINISTRATION
Headquarters, Washington, D.C.

Contract No. NASW-3327

Laboratory Operations
THE AEROSPACE CORPORATION

Aerospace Report No.
ATR-81(7875)-2

ELECTRODYNAMIC STUDIES OF UPPER AND LOWER ATMOSPHERIC COUPLING

Prepared by

Y. T. Chiu, J. M. Cornwall,
B. C. Edgar, M. Schulz, and L. R. Sharp
Space Sciences Laboratory
The Aerospace Corporation

1 March 1981

Laboratory Operations
THE AEROSPACE CORPORATION
El Segundo, California 90245

Prepared for

NATIONAL AERONAUTICS AND SPACE ADMINISTRATION
Headquarters, Washington, D. C.

Contract No. NASW-3327

Report No.
ATR-81(7875)-2

ELECTRODYNAMIC STUDIES OF UPPER AND LOWER ATMOSPHERIC COUPLING

Prepared

Y. T. Chiu

J. M. Cornwall

B. C. Edgar

M. Schulz

L. R. Sharp

Approved

J. M. Straus, Head
Atmospheric Sciences Department

G. A. Paulikas, Director
Space Sciences Laboratory

CONTENTS

I. INTRODUCTION

This report summarizes the principal findings of the theoretical and data-interpretation work performed under NASA Headquarters contract NASW-3327 during the performance period January 1980 to December 1980. The main body of this report is primarily devoted to an overview of the contract work in the various electrodynamical areas of upper and lower atmosphere coupling. Scientific papers published, in press or abstracts of papers in preparation are listed as exhibits in the latter part of this report. The readers interested in detailed scientific findings are referred to the exhibits. Some of the exhibits refer to papers in the final stages of preparation as this report is being prepared. For such papers, full or partial support under this contract will be explicitly acknowledged.

Work performed under the subject contract in the following four areas of electrodynamical studies in upper and lower atmosphere coupling are:

1. Magnetosphere-ionosphere-atmosphere coupling in auroral electrodynamics (3 papers).
2. Middle atmosphere electrodynamics (1 paper).
3. Thermosphere-troposphere coupling (1 paper).
4. Tropospheric electrodynamics (progress report).

Observational and theoretical understanding of the near-earth space environment have progressed in recent years to the point where it is now possible and desirable to find out the interrelationships between various components of the earth's atmosphere. In short, it is increasingly evident that the division of the earth's atmospheric environment into sharply defined

non-interacting spheres has served its earlier function of conceptual simplification and must now be reexamined in regard to the earth's atmospheric response to solar stimuli.

The major tasks detailed for the present study are primarily investigations-in-depth of studies which seem to be most fruitful in the exploratory work of a previous contract, NASW-3120. Studies of ionosphere-magnetosphere coupling in the aurora is a prime example. However, new and unique areas of observations bearing on the electrodynamics of the atmosphere have not been ignored. Items 2 and 4 above are such examples. In the area of auroral electrodynamics, investigations under the present and previous contracts have in some sense borne fruit. Work performed under NASW-3120 and NASW-3327 (the present contract) was the basis from which a full-scaled study of auroral electrodynamics at the Space Sciences Laboratory and UCLA was organized. This study is presently performed under the auspices of NASA's Solar-Terrestrial Theory Program.

II. AURORAL ELECTRODYNAMICS

As a result of work performed under this contract and its predecessor NASW-3120, we were invited to give a review talk, entitled "Effects of Auroral-Particle Anisotropies and Mirror Forces on High-Latitude Electric Fields" (Chiu, Cornwall and Schulz), at the 1980 Chapman Conference on Formation of Auroral Arcs in Fairbanks, Alaska. The conference is sponsored by the American Geophysical Union and the paper will be part of an AGU monograph (ed. S-I. Akasofu) on the formation mechanisms of auroral arcs.

Auroral arcs result from the acceleration and precipitation of ring current and/or plasma-sheet plasma in narrow regions characterized by strong electric fields both perpendicular and parallel to the earth's magnetic field. The various mechanisms that have been proposed for the origin of such strong electric fields are not mutually exclusive. However, for most proposed mechanisms (with the possible exception of double layers of Debye length parallel scale), the effects of auroral particle anisotropy, of mirror forces due to the inhomogeneous geomagnetic field, of auroral electron back-scatter by the atmosphere, and of electron trapping by the combination of magnetic mirroring and electrostatic forces must be taken into account in simulations of auroral electric fields. In addition, the effects of the very strong perpendicular electric field must also be taken into account in a kinetic description of the Poisson equation in order to achieve a unified theory of the auroral electrostatic structure. In this paper, progress in these areas in the past few years will be reviewed. It is shown that particle anisotropies and mirror forces can account for most electrostatic features of the quiet arc, while additional effects may be taking place in strong events in which the parallel potential drop exceeds ~10 kV.

A basic problem of all mechanisms of electrodynamic coupling between upper and lower atmospheres concerns how electric fields are transmitted between the magnetosphere and the atmosphere. In the technical jargon of the field, this is known as electric field "mapping". If magnetic field lines were also electric equipotentials (i.e., no potential drop along the magnetic field line), the "mapping" of electric fields is a simple geometrical procedure dictated by the magnetic field configuration only. However, as

can be seen from the review summary above, there exists a parallel potential drop in the auroral region; thus, the mapping problem takes on entirely different forms. We have made an in-depth study of this problem in a paper entitled "On the Structure of Auroral Acceleration Potentials" (Chiu, Newman and Cornwall). At the time of preparing this final report, this paper is going through the final stages of preparation; therefore, we shall include only the title and summary abstract in this report. Support from NASW-3327 will be acknowledged.

We examine the self-consistency of magnetospheric and ionospheric boundary conditions of a kinetic model of magnetospheric-ionospheric electrodynamical coupling in the aurora formulated by Chiu and Cornwall (1980). This model includes the kinetic current conservation model of Lyons (1980); but in addition, it demands self-consistency between kinetic charge distributions and the divergence of the electric field in accordance with Poisson's equation. It is found that the structures of the ionospheric electric potential in response to imposed magnetospheric structure takes a variety of shapes in agreement with the "V-shaped" and "S-shaped" structures measured by electric field measurements on board the S3-3 satellite. In the absence of a parallel potential drop, the "mapping" of electric fields from the magnetosphere to the ionosphere is strictly dictated by the geometry of the magnetic field. With the presence of a kinetic model parallel potential drop, the "mapping" of electric fields between the magnetosphere and ionosphere is formulated here in terms of our Green's function treatment. It is shown that the new "mapping" filters out structure scales larger than an inverted-V scale (50-150 km) determined by the ionospheric Pedersen conductivity. All structure

scales smaller than this natural scale can be "mapped through" from the magnetosphere to the ionosphere.

Aside from the above two papers, we have also completed the major part of the scientific work on a theory of auroral arc pulsation (Chiu and Cornwall). We show that ion heating by electromagnetic ion cyclotron waves partially destroys the auroral acceleration electric potential, giving rise to a relaxation oscillation of the auroral potential structure. At the time of preparation of this final report, the scientific calculations have been completed but the paper is not yet completely written. Partial support under this contract will be acknowledged.

III. MIDDLE ATMOSPHERE ELECTRODYNAMICS

A major problem in middle atmosphere electrodynamics is how thunderstorm electric fields propagate. For radio frequency electric fields, the problem is well-understood. The problem for electrostatic fields has also been investigated fairly completely in the last few years, due to interest in electrodynamic upper and lower atmosphere coupling. However, because the natural electrodynamic time constant in the middle atmosphere is a few seconds, the significant phenomenon in middle atmosphere electrodynamics is the propagation of sferics of a few second time constant. Data in this area have only recently been obtained with electric field measurements on stratospheric balloons.

As a result of our observational and theoretical efforts, we have been invited to write a chapter, entitled "Sferics in the Stratosphere" (Holzworth and Chiu), in the Handbook of Atmospherics, edited by H. Volland.

This book is under production at the time of preparation of this report. The theoretically predicted features of middle atmospheric sferics are in good agreement with observations. The essential point of this study is that interpretation of middle atmospheric electric field data must take into account propagation effects because the time constant for these effects can be quite long compared to the time constants of possible sources of such electric fields, whether they are of tropospheric or ionospheric origin.

IV. THERMOSPHERE-TROPOSPHERE COUPLING

We have continued compilation of a comprehensive data set of thermospheric density measurements from cold-cathode ion gauges on Atmospheric Explorer and USAF satellites. Fluctuations of these density profiles in the thermosphere are assumed a priori to be signatures of thermospheric gravity waves. We have been interested in correlating features of this data set to physically plausible features of the troposphere as a means of studying upper and lower atmosphere coupling by wave propagation. Under NASW-3120, a paper was published on correlation of thermospheric wave structures with seasonally intense regions of deep tropospheric convective activity indicated by satellite-observed lightning frequency. In our present study, a paper is to be published (essentially accepted) on a correlation of thermospheric wave occurrence with transient tropospheric activity indicated by the vorticity area index (VAI).

Based on the occurrence frequency of thermospheric wave structures in some 24,000 measurements of density, we demonstrate that there is no significant hemispherical correlation between thermospheric waves and the

tropospheric vorticity area index in the epoch 1974-1976. Further, wave occurrence frequency does not exhibit the characteristic feature of the VAI in relation to interplanetary magnetic sector boundary crossings. In the polar zone, (60° - 90°) N, wave occurrence frequency does increase significantly if the hemispherical VAI increases above ~ 30×10^5 km^2. In contrast to previous work (Rice and Sharp, 1977; Chiu et al., 1979), which correlated thermospheric wave occurrence to geographically and seasonally persistent features of the troposphere, this work focuses upon the study of transient (weather) systems as represented by the VAI. Consequently, the null relationship between VAI and the wave occurrence frequency outside the polar zone may reflect the dominance of the persistent sources in the non-polar troposphere.

V. TROPOSPHERIC ELECTRODYNAMICS

Due to delays in the delivery of global lightning sensor data from Aerospace instruments on board two DMSP satellites, we have not been able to complete acquisition of enough statistics until late in the year to correlate global lightning occurrence with solar and galactic cosmic ray events. Exploration for such possible connections with high statistics data is prompted by recent speculation that mesospheric and tropospheric electrodynamics may have some relationship to nucleation around increases of seed ionization or to the global electrical circuit.

By September 1980, however, data delivery difficulties have been ironed out; and, we have been able to analyze the following set of lightning data which involve interesting solar-galactic cosmic ray events and global lightning events:

Data Periods: Sep. 6-30, 1977

Nov. 7-12, 1977

22-30, 1977

Feb. 13-24, 1978

Apr. 6-26, 1978

Nov. 2-30, 1978

Apr. 3-30, 1979

May 1-7, 1979

15-28, 1979

Aug. 14-28, 1979

The selection criteria of these data periods are: 1) existence of cosmic ray events during the periods, and 2) existence of essentially continuous global lightning data from our instruments.

At the time of preparing this final report, we have completed analysis of the above data set. A quick-look analysis shows that indeed there are some distinct coincident events that are more than 1σ over the statistical average, but the total picture seems to be much more complex. We shall make a careful assessment of the statistical significance of the quick-look results. NASW-3327 will be acknowledged in our publications as a mainstay of support in this analysis. We plan to present the results of the analysis in the spring of 1981.

VI. CONCLUSIONS

Our research work, in a year's time, has spanned virtually the entire spectrum of currently interesting areas of electrodynamical studies

in upper and lower atmosphere coupling. Clearly, our findings cannot be said to have proved the existence of an incontrovertible coupling mechanism between the magnetosphere and troposphere. However, the work on magnetosphere-ionosphere coupling, when compared with observations, indicates that, indeed, electrodynamics are the key mechanism in which the ionosphere actively participates in the precipitation of solar wind energy into the high-latitude atmosphere. There, something mysterious happens, so that occurrence statistics of thermospheric turbulence in the form of gravity waves at high latitudes is somehow correlated with tropospheric transient turbulence as indicated by the vorticity area index. We cannot as yet determine whether this correlation is entirely due to tropospheric driving or is "helped along" by the special electrodynamical conditions set up in the high-latitude region. In this regard, it is of interest to note that the high-latitude zone (> 60° latitude) is mostly outside of the most violent zone of tropospheric transient turbulence, the front of "polar" air masses.

To find out the possible physical mechanisms, which may be responsible for such "mysterious" correlations, we feel that the most potentially rewarding area of new research contributions may be in middle atmosphere electrodynamics. The theoretical concepts and methods in this area have yet to be tested by electrodynamical measurements on stratospheric balloons and, in the near future, on mesospheric satellites. Our contract work in this area has demonstrated that some element of theoretical interpretation of such data can be understood. We intend to pursue this area of research in co-ordination with balloon and satellite programs of mesospheric and stratospheric electrodynamics.

The scientific papers (published, in press, accepted for publication or in preparation), which are attributed to support by NASW-3327, are listed in the following. The actual papers, presently available, are attached at the end of this report as exhibits.

1. Effects of auroral-particle aniosotropies and mirror forces on high-latitude electr · fields, Y. T. Chiu, J. M. Cornwall, and M. Schulz, Invited paper, 1980 Chapman Conference on Formation of Auroral Arcs, Fairbanks, Alaska. To appear in AGU monograph 1981, ed. S.-I. Akasofu.
2. Sferics in the stratosphere, R. H. Holzworth and Y. T. Chiu, Chapter 16, Handbook of Atmospherics, ed. H. Volland, in production, 1980.
3. Correlative study of thermospheric gravity waves and tropospheric vorticity area index, Y. T. Chiu and L. R. Sharp, Geophysical Research Letters, 8, 281, 1980.
4. On the structure of auroral acceleration potentials, Y. T. Chiu, A. L. Newman and J. M. Cornwall, in final stages of preparation and to be submitted to J. Geophys. Res., 1981.
5. Theory of auroral arc pulsation, J. M. Cornwall and Y. T. Chiu, in preparation and to be submitted to J. Geophys. Res., 1981.

Exhibit A: Effects of Auroral-Particle Anisotropies and Mirror Forces on High-Latitude Electric Fields, by Y. T. Chiu, J. M. Cornwall and M. Schulz

EFFECTS OF AURORAL-PARTICLE ANISOTROPIES AND MIRROR FORCES ON HIGH-LATITUDE ELECTRIC FIELDS*

Y. T. Chiu, J. M. Cornwall**, and Michael Schulz

Space Sciences Laboratory
The Aerospace Corporation
P. O. Box 92957
Los Angeles, CA 90009

**Permanent Address: Department of Physics,
University of California, Los Angeles, CA 90024

Abstract

Auroral arcs result from the acceleration and precipitation of ring current and/or plasma-sheet plasma in narrow regions characterized by strong electric fields both perpendicular and parallel to the earth's magnetic field. The various mechanisms that have been proposed for the origin of such strong electric fields are not mutually exclusive. However, for most proposed mechanisms (with the possible exception of double layers of Debye length parallel scale), the effects of auroral particle anisotropy, of mirror forces due to the inhomogeneous geomagnetic field, of auroral electron backscatter by the atmosphere, and of electron trapping by the combination of magnetic mirroring and electrostatic forces must be taken into accoun ı simulations of auroral electric fields. In addition, the effects of the very strong perpendicular electric field must also be taken into account in a kinetic description of the Poisson equation in order to achieve a unified theory of the auroral electrostatic structure. In this paper, progress in these areas in the past few years will be reviewed. It is shown that particle anistropies and mirror forces can account for most electrostatic features of the quiet arc, while additional effects may be taking place in strong events in which the parallel potential drop exceeds ~ 10 kV .

*Invited Paper: 1980 Chapman Conference on Formation of Auroral Arcs, 21-24 July 1980, Fairbanks, Alaska

This work is supported by NASA under Grant NASW-3327.

I. INTRODUCTION

The latter half of the nineteen seventies has witnessed a spectacular increase in the understanding of the electrodynamics of the auroral arc. This happy circumstance is supported on the one hand by the advent of simultaneous high-resolution particle and field observations at altitudes of ~ $1R_E$, such as those obtained by instruments on board the S3-3 satellite, and on the other hand by earlier rocket and radar backscatter observations at ionospheric altitudes. Although the optical aurora has stirred human imagination since time immemorial, it is perhaps not an exaggeration to say that only now are human beings able to grasp an outline of the mechanisms for the formation of the auroral arcs themselves. As we may reasonably expect, the observations indicate a complex but basically electrodynamical interaction between plasma particles and fields (electric as well as magnetic) in the auroral magnetosphere.

In this paper, we shall undertake to review certain unavoidable, indeed "inevitable", aspects of the electrodynamical interaction between particles and fields in the auroral region of the magnetosphere. These effects, which conspire to support an electric potential drop along auroral field lines to accelerate magnetospheric electrons downward and ionospheric ions upward, are "inevitable" in the sense that they are imposed by the following unavoidable external circumstances: the mirroring motion of particles in the earth's dipole-like magnetic field, the differential anisotropy of injected plasma-sheet electrons and ions, the existence of the ionosphere with the inevitable implication of electron backscatter and current closure, and, last but not least, the existence of large electric potential drops perpendicular to the magnetic field. We shall show that an integrated model of these "inevitable" factors can account for the recent satellite observations of particles and fields in the quiet auroral arc (observed on the day-to-day basis). It is not our intention in this review to treat the electrodynamics of complex spectacular auroral events in which electron energies are greater than a few kilovolts.

Although the specific purpose of this brief review is to address the effects of the above-mentioned factors in auroral dynamics, it would be unphysical to discuss these factors without considering their relationship to observations and to the theoretical interpretation of those observations. In

particular, we need to clarify the relationship of these "inevitable" effects to present electrodynamical theories of the formation of auroral arcs; thereby, we hope to formulate a "unified" model of auroral electrodynamics. For these reasons, brief reviews of observations and data interpretation will be included here.

In a brief review such as this one, it is inappropriate to give an exhaustive reference list; therefore, we shall attempt to give only a representative reference list, emphasizing the latest results, so that the reader can trace a more complete reference if he so chooses. Thus, works referenced here are not necessarily judged by us to be of special significance; similarly, works not referenced here are not judged to be comparatively any less significant.

II. OBSERVATIONS

Before the advent of high-resolution observations by auroral satellites, data on ionospheric and magnetospheric coupling depended on balloon, rocket, and radar observations which were necessarily episodic; nevertheless, the basic physical properties of auroral ionospheric currents and electric fields (e.g., Cloutier, 1971; Mozer and Manka, 1971; Vondrak et al., 1971), together with their relationship to high-latitude convection electric fields (e.g., Cauffman and Gurnett, 1972; Heppner, 1972) measured by satellites, have been established. Generally, these measurements have indicated that the substorm convection electric field in the magnetosphere drives perpendicular ionospheric currents consistent with ionospheric perpendicular electric fields (meridional and zonal) of the order of tens of millivolts/meter. In addition, Birkeland currents parallel to auroral magnetic field lines seem to have been observed (e.g., Armstrong and Zmuda, 1973). These low-altitude observations are primarily concerned with the morphology and large-scale processes of auroral substorms and are instrumental in emphasizing the importance of the electric field in auroral processes. They, however, have relatively little to say about the microscopic processes taking place in the auroral region.

Even as the large-scale auroral processes were being unraveled, certain microscopic features of auroral low-energy particle precipitations were being discovered. Frank and Ackerson (1971) noted that occasionally observations of low-energy (tens of keV) electron precipitation would show an "inverted-V"

structure on an energy-time spectrum plot, i.e., the precipitating electron energy spectrum hardens and then softens as the Injun 5 satellite moves through the structure. Evans (1974; 1975) convincingly demonstrated that rocket measurements of auroral low-energy electrons indicated downward moving electron beams at keV energies, comparable to those of "inverted-V" structures. Further, by a careful study of electron backscatter from the atmosphere, Evans demonstrated that these auroral electron beams are indications of electric potential drops, along the magnetic field, existing between the equator and the ionosphere. At about the same time, observations of singly ionized energetic O^+ ions in the magnetosphere (Shelley et al., 1972; Sharp et al., 1974) also gave indication that microscopic processes in the aurora couple the ionosphere with the magnetosphere.

These observations of "inverted-V" structures, of electron beams, and of O^+ ions of probable ionospheric origin in the magnetosphere presage very interesting microscopic processes to be discovered in the auroral process in which the ionosphere plays an active rather than passive role. However, because of the episodic nature of rocket observations and because of the low resolution and low data rate of the early satellite observations, the scope of and inter-relationship between these phenomena were not understood until the launch of the polar-orbiting auroral satellite S3-3, which intercepts auroral field lines at altitudes up to ~ 8000 km , precisely in the region where ionospheric and magnetospheric plasmas are expected to interact. Included in the S3-3 payload are instruments to measure electric fields (Mozer et al., 1977), low energy electrons (Mizera et al., 1976), energetic ions (Shelley et al., 1976), and plasma waves (Kintner et al., 1978).

The S3-3 observations not only confirmed Evans' observations of downward-moving field-aligned electron beam at keV energies but also revealed the existence of upward-moving ion beams aligned with the magnetic field in "inverted-V" structures. This certainly indicates that the three phenomena are intimately related, but more importantly the S3-3 particle observations leave little doubt that an electric potential drop of several to tens of kilovolts, aligned with the magnetic field, exists between the ionosphere and the magnetospheric equator. Electrostatic field measurements also indicate paired regions of oppositely directed perpendicular electric fields, with latitudinal scale lengths of some 50 km, reflecting a negative space-charge region pre-

sumably associated with downward-streaming electrons. Figure 1 which is a composite of particle and electric field data illustrates the above points. For further emphasis, Figure 2 shows an enlarged view of the perpendicular electric field data for the time period marked by the brace in the middle of Figure 1. A crucial, but seldom emphasized, feature which is brought out by the high sensitivity and high resolution of the S3-3 measurements is that the above correlated features are observed at the auroral zone pass after pass at all satellite altitudes. In other words, these are fundamental features of the aurora rather than episodic curiosities.

III. THEORETICAL INTERPRETATIONS

The key theoretical issue concerning the interpretation of the S3-3 observations really involves the electrodynamics of the auroral arc itself. A key fact which must be recognized is that a magnetic-field-aligned electrostatic potential difference of kilovolt magnitude exists between the ionosphere and the equator. In many respects, this feature has been anticipated in a number of theoretical considerations based on earlier observations. The crucial question is whether the mechanism for the buildup of such a field-aligned potential drop involves the ionosphere, for there is no doubt that the energy source of the aurora is derived from the interaction between the solar wind and the magnetosphere via plasmas which are injected by substorm processes onto the auroral field lines. Some aspects of the theories of auroral field-aligned potential drop have been reviewed (Shawhan et al., 1978; Hudson and Mozer, 1978), but our discussions will be primarily concerned with the particle anisotropy and particle mirroring aspects of these theories.

Theories of auroral processes involving magnetic-field-aligned electrostatic potential differences can be roughly classified into five categories, although they are not mutually exclusive. These are: 1) Debye-length double layer, 2) oblique electrostatic shock, 3) anomalous resistivity, 4) downward mapping of convection electric field discontinuities, and 5) magnetic mirroring effects of differential pitch-angle anisotropy between ions and electrons. These categories invoke theoretical arguments of varying degrees of sophistication and believability to show that kilovolt electrostatic potential drops may be produced in various assumed plasma distributions. The Debye-length double-layer model is sharply differentiated from the others by

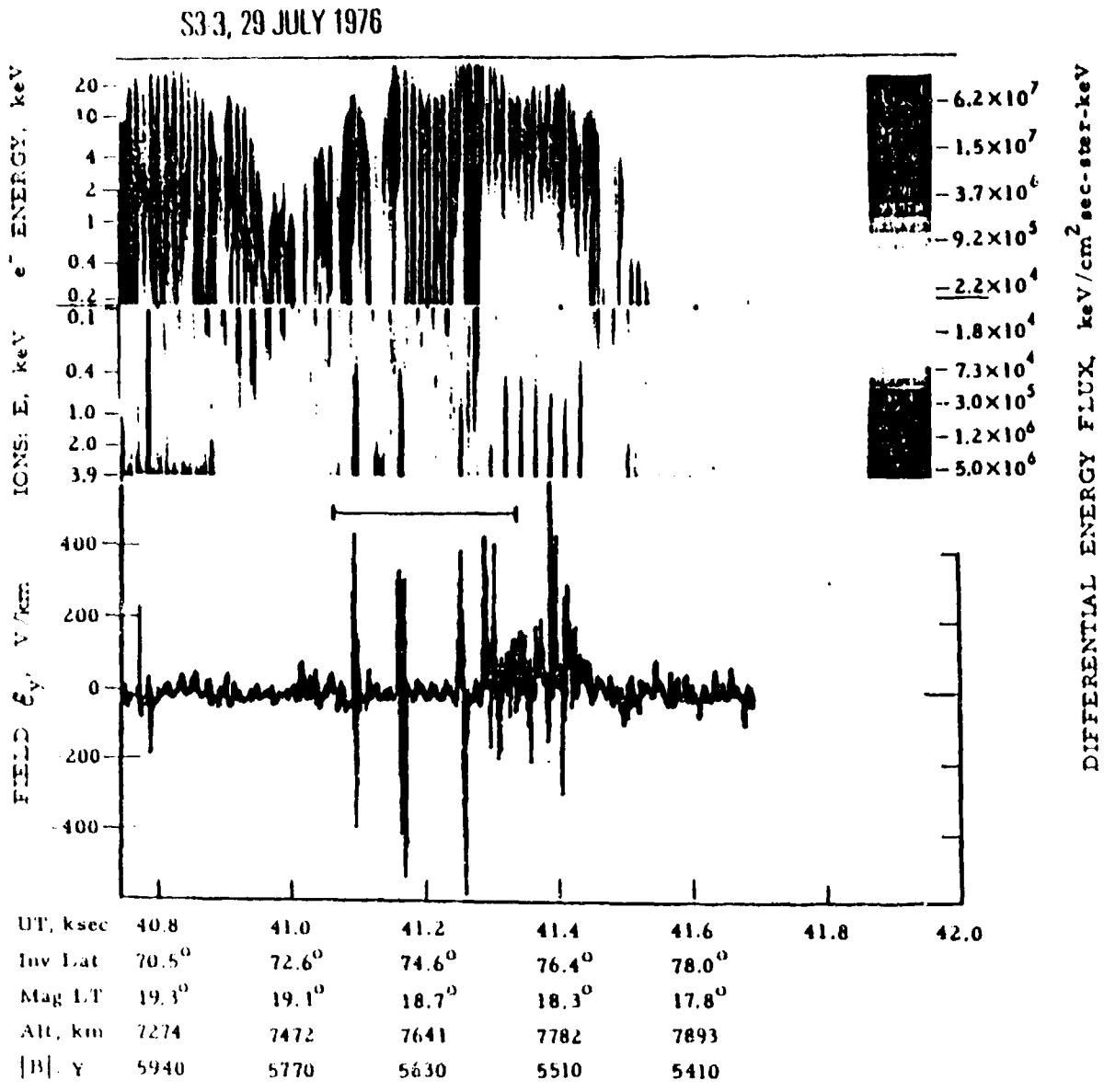

Fig. 1. Simultaneous observations of electron energy spectrum, ion energy spectrum and perpendicular electrostatic field structures on July 29, 1976, by the S3-3 satellite. (Courtesy F. S. Mozer, R. B. Torbert, P. F. Mizera and J. F. Fennell.)

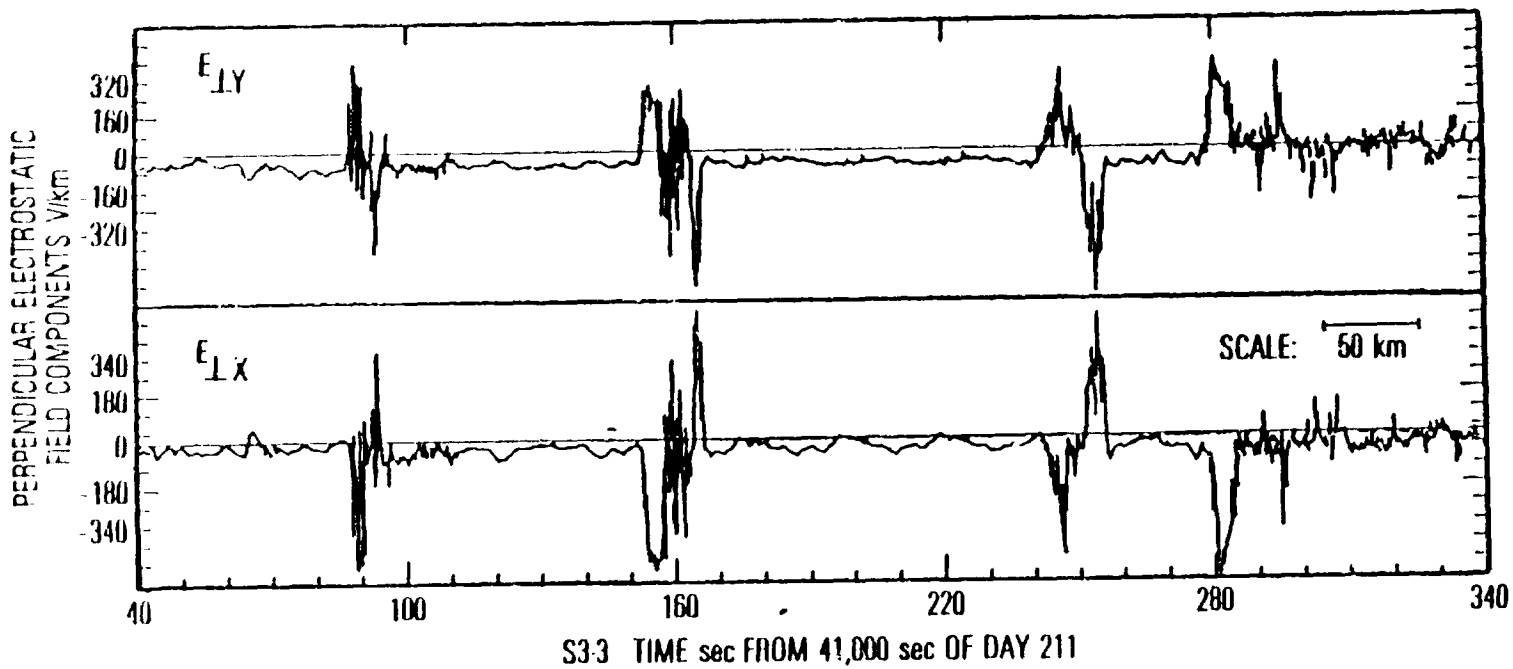

Fig. 2. Expanded view of the two perpendicular components of the electrostatic field for the period indicated by the brace in the middle of Fig. 1. (Courtesy F. S. Mozer and R. B. Torbert.)

its prediction of the scale length with which the total field-aligned potential difference is distributed, i.e., the magnitude of the parallel electric field.

Our brief discussion begins with the traditional view of these mechanisms in isolation; then we shall proceed to consider their relationship to the effects of particle dynamics mentioned in the Introduction.

The Debye-length double layer (Block, 1975; Shawhan et al., 1978) is a boundary layer between unmagnetized cold plasma on one side and hot plasma on the other. The potential drop across the layer is alleged to be $\sim kT_e/|e|$ and the layer thickness is of the order of several Debye lengths (~ 10 km); thus, the parallel electric field in double layers must be ~ (0.1 - 1) V/m. A current-driven instability is usually invoked as the formation mechanism of double layers, which requires a field-aligned current greater than a certain threshold value. If potential drops inferred by electron beam observations at S3-3 altitudes as high as ~ 8000 km are all due to double layers above the satellite, then evidently the ionosphere does not seem to be a factor in double layer formation. Frequently, based on observations of both electron and ion beams on S3-3, one may infer that potential drops exist both above and below the satellite (Mizera and Fennell, 1977; Croley et al., 1978). Since it is highly improbable that the satellite just happened to pass through within the double layer thickness, such frequent occurrences seem to require more than one double layer to be formed on the same field line. Further, given the small scale length of the layer, it would be rather difficult for the mechanism to explain the coincident observation of downward electron beams and upward O^+ beams unless the double layer occurs at the topside ionosphere where O^+ is plentiful. Theories of double layer formation are mathematically difficult, even for very simple plasma distributions (Montgomery and Joyce, 1969), and a quantitative theory has yet to be developed for auroral plasmas in an inhomogeneous magnetic field. For these reasons, we shall not discuss the possible relationship between Debye-length double layers and the effects of particle anisotropies and mirror forces, although the latter are bound to enter into consideration of Debye-length double layers in magnetized plasmas.

Oblique electrostatic shocks (Swift, 1975; 1976; Kan, 1975) are similar to double layers except that they recognize the influence of the magnetic

field and consider that the shock normal is at an arbitrary angle α to the magnetic field direction. For $\alpha \neq 0$ the shock thickness ℓ is measured in units of the ion gyroradius of a few km, a typical cross-field scale being some 15-20 gyroradii (~ 100 km). The field-aligned scale length is $\ell/\cos\alpha$ which can be quite extensive if the shock normal angle α approaches $\pi/2$. Swift has shown that self-consistent oblique shock solutions to Poisson's equation can be obtained with simple plasma distributions in an inhomogeneous magnetic field (Swift, 1979). The oblique shock geometry has certain advantages over the current-driven double layer in regard to the interpretation of S3-3 data, even though the theory was conceived prior to S3-3. This is because the field-aligned scale length $\ell/\cos\alpha$ can be chosen to be of the order of 1-2 R_e so that only one shock (or a pair of double reverse shocks) need be invoked to explain the existence of potential drops above and below the satellite. It is, of course, a disadvantage that the theory as developed by Swift does not predict α , or equivalently the cross-field scale length. As we discuss later, this scale length can be estimated by incorporating ionospheric physics. An oblique shock with parallel scale length ≥ 1 R_e is almost certainly strongly coupled to the ionosphere, which at the very least supplies important boundary conditions for the shock. Presently, there seems to be some controversy concerning the distinction between electrostatic shocks and "double layers" of all parallel scales (Goertz, 1979; Kan, 1980). These arguments do not concern us; here we adopt the terminology of the initial author in order to maintain impartiality.

A third mechanism by which a magnetic-field-aligned electric potential drop can allegedly be generated is anomalous resistivity in the field-aligned direction (Hudson et al., 1978). Such anomalous resistivity may be due to a large number of possible modes of AC electric-field turbulence in the auroral plasma (e.g., Kindel and Kennel, 1971; Papadopoulos and Coffey, 1975). Hudson et al. (1978) estimated that turbulent electric fields in the electrostatic ion cyclotron mode with amplitudes ~ 50 mV/m may yield sufficient anomalous resistivity to generate parallel electrostatic (DC) fields of ~ 1 mV/m. It is not clear how the largely perpendicular AC fields can affect parallel electron currents (and their resistivity). One feature common to oblique-shock models and anomalous-resistivity models is that the potential smoothly varies over a scale of ~ 1 R_e extension in order to accommodate potential drops of ~ (1-10) kilovolts. It must be noted that the question of how such an

extensive region of turbulence can be maintained at a high level (~ 50 mV/m AC), in the presence of non-linear stabilizing effects such as ion heating, must be addressed. However, to address this question, it seems to us that the effects of particle motion in an inhomogeneous magnetic field and the effects of ionospheric plasma cannot be ignored. Further, to study the generation of the electrostatic turbulence, the ultimate cause must be looked for in the characteristics of particle distribution functions. Again, we find ourselves returning to the question of particle distributions in an inhomogeneous magnetic field.

The fourth source of auroral electric fields that accelerate ions and electrons in opposite directions along the earth's magnetic field is the magnetospheric convection electric field. The convection electric field is perpendicular to the magnetic field at high altitudes, but its meridional (r,θ) component has a theoretical discontinuity at or near the boundary between closed and open magnetic field lines. Figure 3 shows the amplitudes of the diurnal variation of $\underline{E}$ at ionospheric altitudes (Chiu et al., 1979; Lyons, 1980). Ionospheric resistivity would partially connect electrostatic equipotentials across the discontinuity, but at too low an altitude to account properly for the observed component of $\underline{E}$ parallel to $\underline{B}$. However, the "kinematical resistivity" associated with magnetic-mirror forces on a hot plasma may increase the altitude at which the parallel (to $\underline{B}$) component of $\underline{E}$ would appear. The details of this latter effect, which (if it occurs) would produce the desired distribution of $\underline{E} \cdot \underline{B}$ with altitude, remain to be worked out in detail. Lyons (1980) has considered the perpendicular distribution of the parallel potential drop in a model incorporating the ionosphere. The effect would be such as to produce an upward electric field in the PM sector (maximal at dusk) and a downward electric field in the AM sector (maximal at dawn) of the auroral oval. This expectation is in good agreement with the diurnal distribution of upgoing ion beams observed by Ghielmetti et al. (1978). However, to study the distribution of $\underline{E}$ parallel to $\underline{B}$, one must again face the question of particle distributions in an inhomogeneous magnetic field.

For the most part, these mechanisms have been considered in isolation of each other and of the ionosphere, not because physicists believe that it should be so, but because it is difficult to treat the couplings. In fact, a correct theoretical treatment of auroral phenomena will without doubt merge

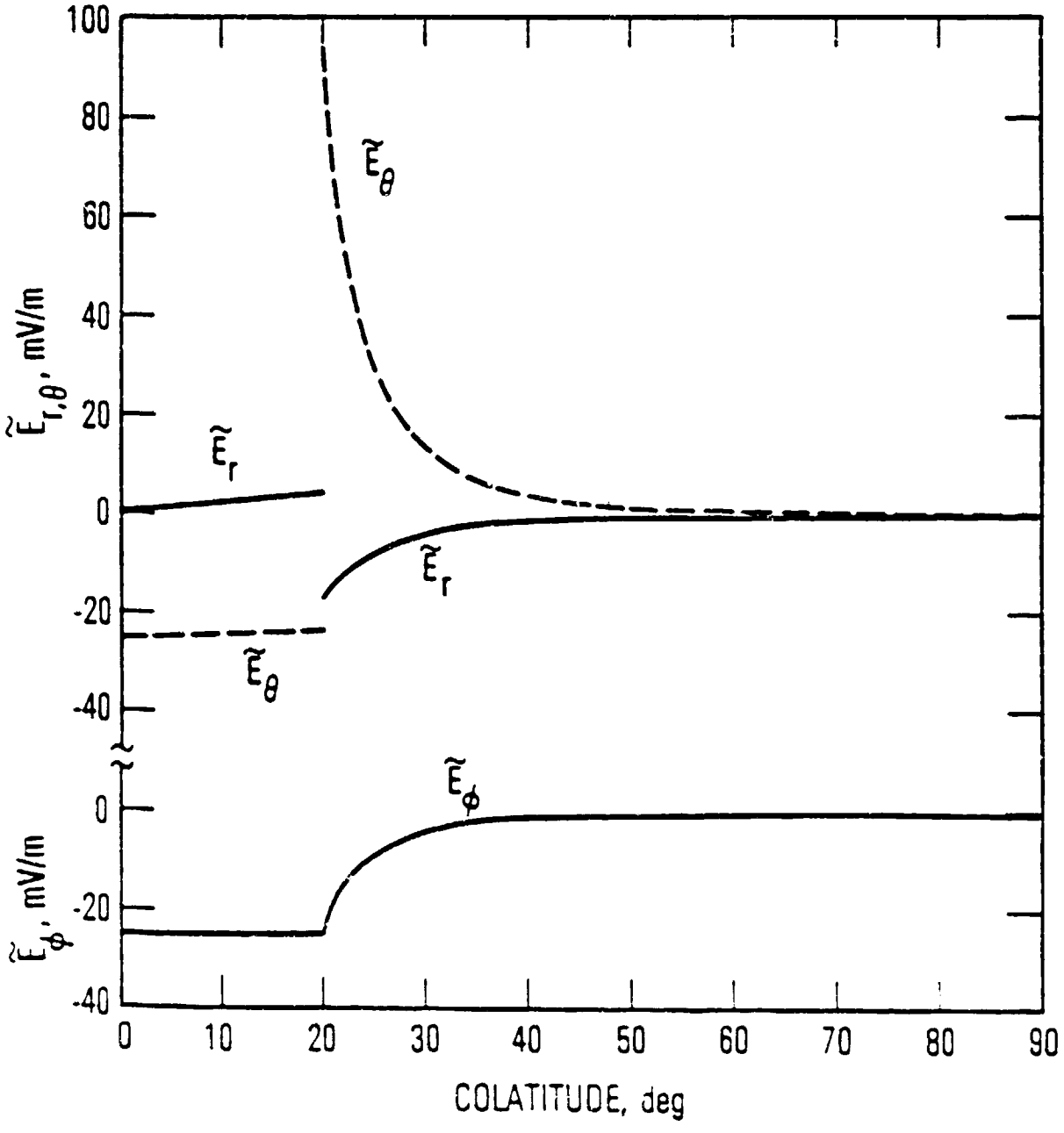

Fig. 3. Amplitudes of the diurnal variation $\tilde{E}$ at ionospheric altitudes.

several of these mechanisms with each other and with ionospheric physics. It is unfortunate that much of the recent literature on auroral mechanisms pays so little attention to coupling with the ionosphere; some exceptions (with two of which the authors are connected) exist, though. As a general rule, the ionosphere couples neighboring field lines and allows for predictions of latitudinal structure and scale lengths. There is no such coupling in the individual mechanisms mentioned above (except that oblique shocks have an arbitrary structure which crosses field lines), so none can explain arc structure without going beyond the given mechanism. The unifying thread running through the above consideration of the mechanisms is, of course, the necessity for establishing the proper self-consistency between particles and field distributions in an inhomogeneous mirroring magnetic field with proper ionospheric and magnetospheric boundary conditions.

It is with the consideration of this common thread in mind that we are led to the effects of auroral-particle anisotropies and mirroring forces on the distributions of electric fields in the auroral region.

IV. PARTICLE ANISOTROPY AND MIRROR FORCES

The effects of particle anisotropies and mirror forces in an inhomogeneous magnetic field have traditionally been considered as a mechanism for generating a parallel potential drop in the same sense as the mechanisms considered above (see, for example, Lemaire and Scherer, 1974; Shawhan et al., 1978; Chiu et al., 1979). However, because these effects owe their existence to "inevitable" factors of magnetic field geometry, ionospheric and magnetospheric boundary conditions, they should properly be discussed apart from "dynamical" mechanisms. These effects do not act in isolation or in opposition to the mechanisms discussed above; rather, as we shall see, they may be the common thread which unifies the various mechanisms (except for the Debye-length double layer) into a single auroral mechanism. Figure 4 shows an example of the difference of pitch angle distributions between ions and electrons observed by instruments on board the SCATHA satellite near the equatorial regions of auroral field lines. So, differential anisotropy between ions and electrons is observed fact, not hypothesis.

As far as we can determine, Alfvén and Fälthammar (1963) were the first to point out that low density two-component mono-energetic plasma in an

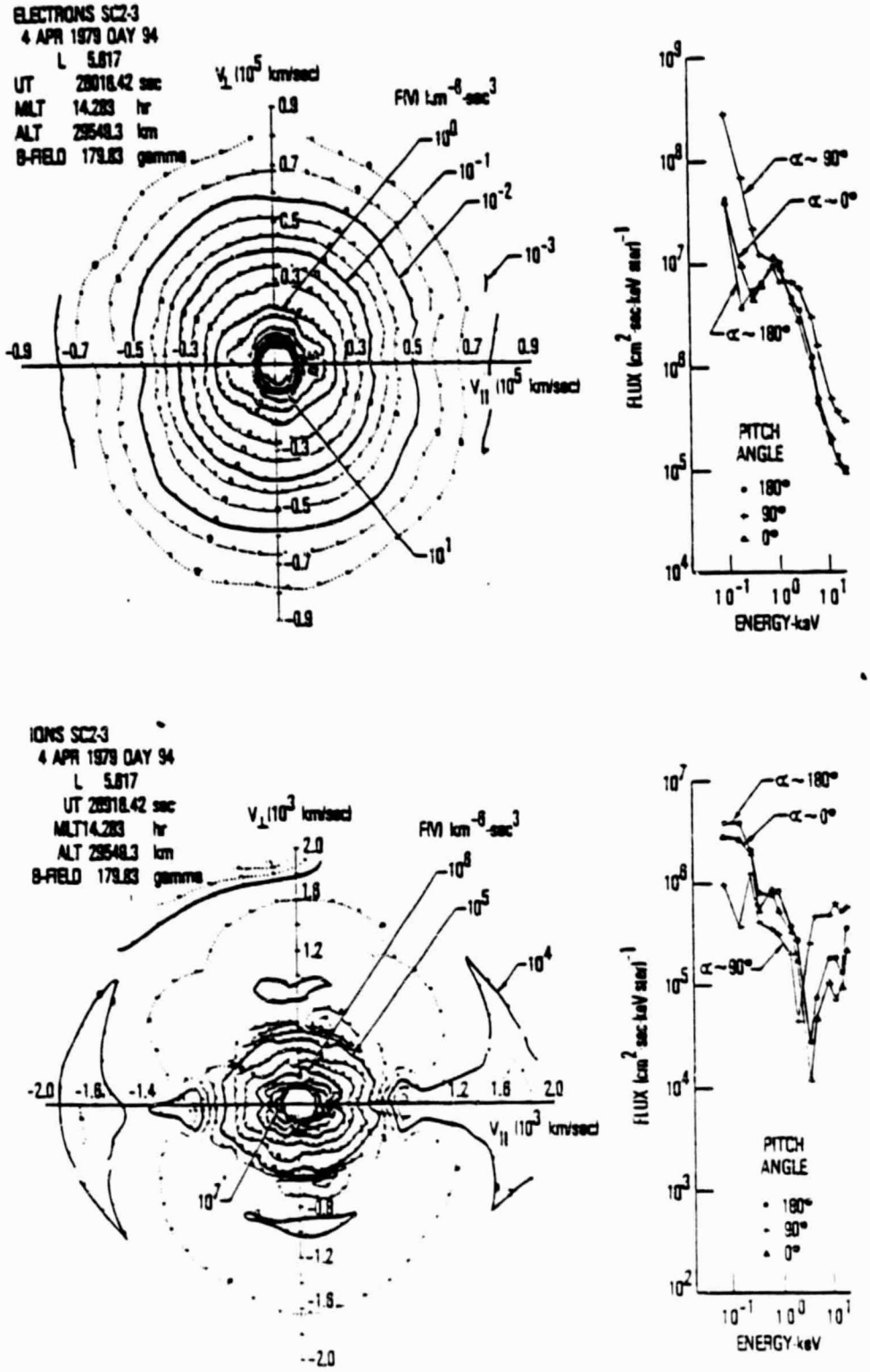

Fig. 4. Pitch angle distributions of ions and electrons near the equatorial regions of auroral field lines. (Courtesy J. F. Fennell and D. R. Croley, Jr.)

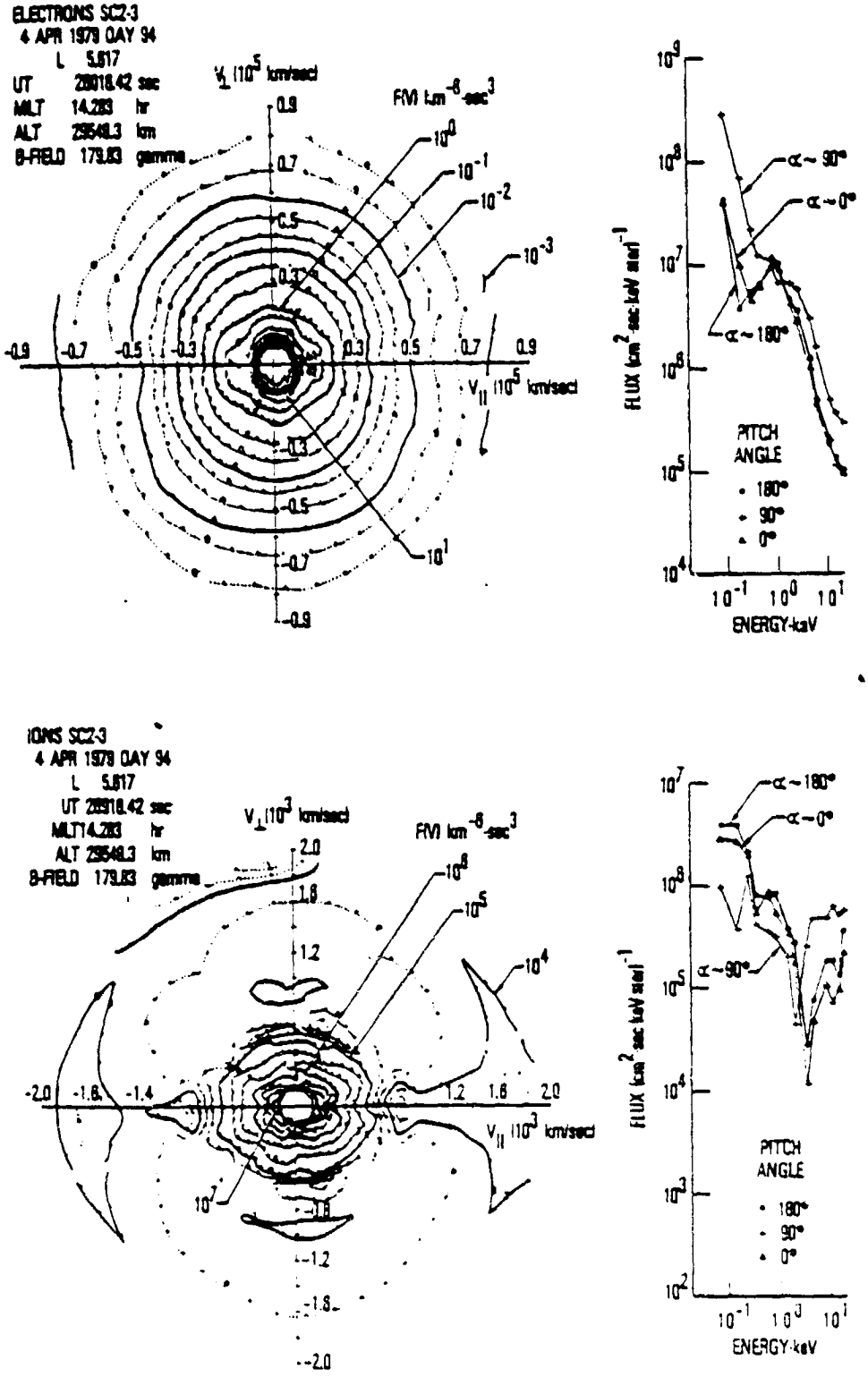

Fig. 4. Pitch angle distributions of ions and electrons near the equatorial regions of auroral field lines. (Courtesy J. F. Fennell and D. R. Croley, Jr.)

inhomogeneous mirroring magnetic field must support a parallel electric field unless the anisotropies of energy (i.e., ratio of parallel to perpendicular kinetic energy) are the same for both ions and electrons. Their results have been further developed by Persson (1966), yielding a potential drop $\Delta\phi$ between the ionosphere and the equator.

$$\Delta\phi = \frac{1}{|e|}\,(B_\ell/B_0 - 1)\quad \frac{w_{i\perp}\,w_{e\parallel} - w_{e\perp}\,w_{i\parallel}}{w_{i\parallel} + w_{e\parallel}} \tag{1}$$

where B is the magnetic field, w is the kinetic energy of the component and species indicated by the subscripts, and the subscripts ℓ and 0 denote the ionosphere and the equator respectively. Since $B_\ell/B_0 \gg 1$ for auroral field lines, $|e|\,\Delta\phi$ would be much greater than the auroral particle kinetic energies (~ 10-100 keV) unless the anisotropy difference between electrons and ions is of order B_0/B_ℓ. Ponyavin et al. (1977) pointed out that the potential drop for a two-component bi-Maxwellian plasma would be much less,

$$\Delta\phi = \frac{2}{|e|}\cdot\frac{w_{\parallel e}\,w_{\parallel i}}{w_{\parallel e} + w_{\parallel i}}\ln\ \frac{1 + (w_{\perp e}/w_{\parallel e})\,x}{1 + (w_{\perp i}/w_{\parallel i})\,x}\quad , \tag{2}$$

where $x = B_\ell/B_0 - 1$, yielding $|e|\,\Delta\phi$ to be about half of the average particle kinetic energy (a few keV). Similar results have also been discussed by Whipple (1977) and Lennartsson (1977).

While the geometrical and boundary-imposed properties of particle distributions are the basic causes of the parallel potential drops discussed above, i.e., ions and electrons of different pitch angle distributions mirror on the average at different locations of the field line thus creating a charge-separation electric field, the above results are arrived at by requiring a parallel potential distribution to maintain a balance of positive and negative charges on a field line (quasi-neutrality). For this reason, the effects of particle anisotropy and mirror forces are quite frequently intermingled with quasi-neutrality - to the extent that these effects have become inseparable from quasi-neutrality. In reality, we must be careful to distinguish quasi-neutrality, which is nothing more or less than an assumed method of deriving

the parallel potential ϕ, from the more basic and "inevitable" factors of particle anisotropy and mirror forces. Indeed, we shall discuss more general applications of these factors in the next section.

The application of quasi-neutrality to obtain solutions of kinetic equilibrium between particles and fields has had a long history. Lemaire and Scherer (1971) have pioneered a series of applications of these kinetic principles to a number of magnetospheric problems involving primarily isotropic Maxwellian distributions. Applications to auroral plasmas have become the dominant topic in recent years (Lemaire and Scherer, 1974; Knight, 1974; Lennartsson, 1977). Chiu and Schulz (1978) reexamined the problem in the light of the S3-3 observations and suggested the necessity of taking into account other "inevitable" factors such as electron backscatter from the ionosphere (eloquently noted by Evans (1974; 1975) a few years earlier) and electron trapping by a combination of electric and mirroring forces. A typical quasi-neutral solution for the equilibrium potential is shown in Figure 5. In general, the parallel electric field due to the factors discussed here is distributed over the entire auroral field line so that the parallel electric field strength is < 1 mV/m. Further, as has been noted in simple model calculations, the more complex models confirm that a potential drop of < 10 kV can be supported by these basic factors of particle kinetics; thus, particle anisotropy and mirror forces cannot account for the more spectacular auroral events in which the potential drop can be as high as 30 kV.

A final aspect of particle anisotropy and mirror forces in auroral dynamics is somewhat subtle and is not generally appreciated. By suggesting that the basic parallel electric field distribution is a direct kinetic consequence of externally imposed geometric and boundary factors, we are also suggesting that there is an "inevitable" kinetic resistivity to the auroral low-density plasma so that dynamical processes such as plasma waves do not play a major role in determining the current-field relationship ("Ohm's law") in the quiet arc. This viewpoint has been expressed as the "kinetic picture" by Lemaire and as the "current-carrying characteristics of the low density auroral flux tube" by Evans. A simple but "inevitable" prediction of this "kinetic picture" is the relationship between field-aligned current $J_{\parallel}$ and the electric potential drop $\Delta\phi$

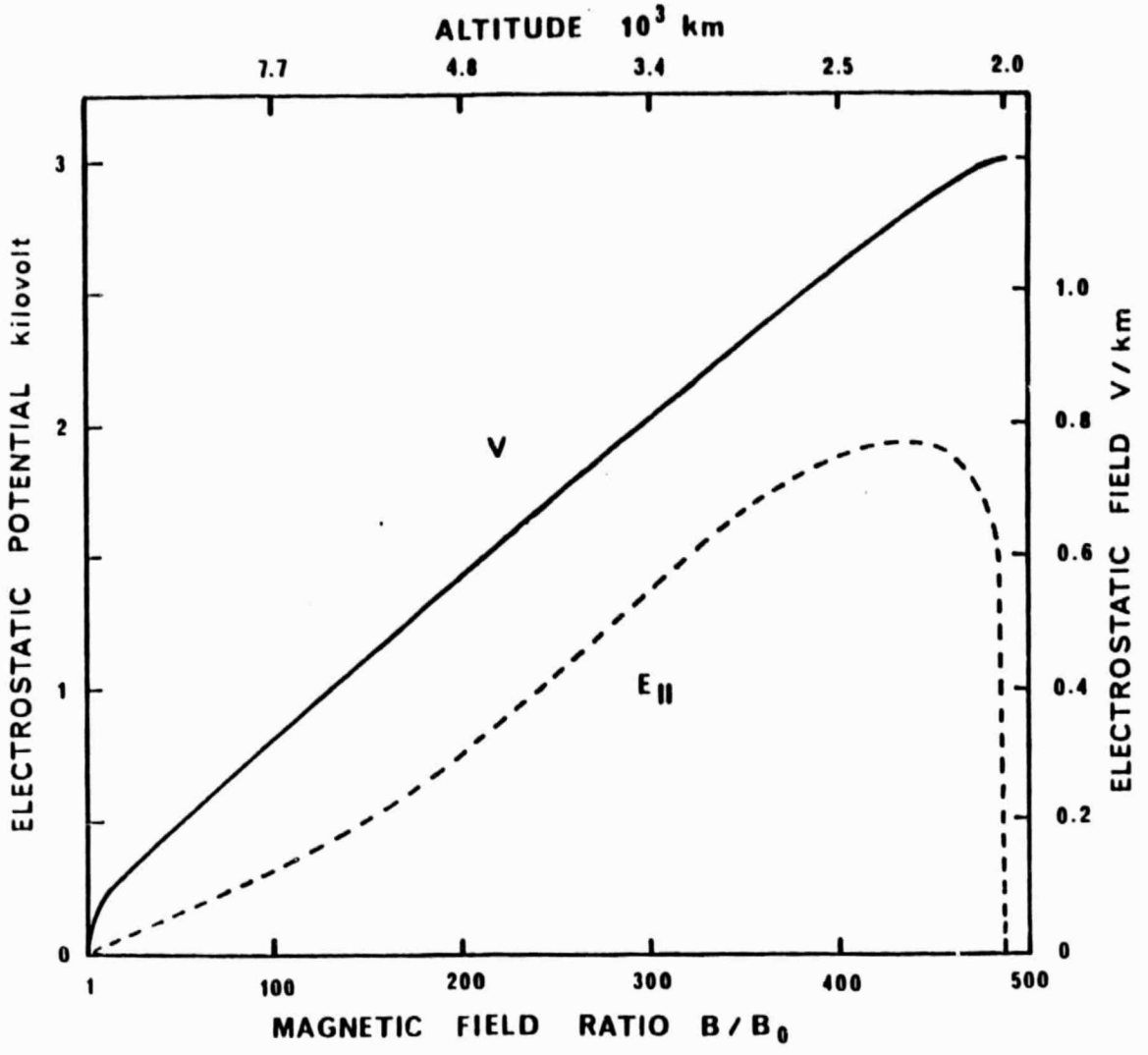

Fig. 5. A typical solution for the parallel potential and electric field for typical ionospheric distributions and assumed potential drops.

$$J_{\parallel} = A\Delta\phi \qquad (3)$$

where A is derivable from the parameters of the particle distribution functions (Fridman and Lemaire, 1979; Chiu and Cornwall, 1980). Lyons et al., (1979) have essentially demonstrated the validity of (3) with observations.

V. TOWARDS A UNIFIED MODEL OF THE QUIET ARC

In Section III, we have noted that the kinematics of particle distributions in the inhomogeneous mirroring geomagnetic field is a common thread which links the various suggested mechanisms for the auroral parallel electric field. In Section IV, we have reviewed the development of this common thread - specifically, the effects of particle anisotropy and mirror forces in quasi-neutral models. Since these effects owe their existence to "inevitable" factors of magnetic field geometry and boundary conditions in the ionosphere and magnetosphere, the next logical step in the development of a model of quiet arc formation would be to consider the various mechanisms (except the Debye-length double layer) in the light of this unifying thread.

It is evident that these physical mechanisms do not exist entirely independently of one another. For example, if the restrictive assumption of strict charge neutrality is removed in the magnetic-mirror model, one has an oblique electrostatic shock in a mirroring field. To the extent that no dissipative mechanisms such as wave-particle turbulence are included in such a "shock", the resulting electric-field structure is better described as a solution of Poisson's equation. From another point of view the oblique shock can be described as some sort of zero-frequency electrostatic ion-cyclotron (ESIC) mode. There surely is a great deal of ESIC turbulence connected with auroras, and the physical distinction between the oblique shocks of Swift and this turbulence is at best imprecise. Yet the merging of wave turbulence and shocks can lead to substantial parallel electric potential drops in the complete absence of anomalous resistivity. (The reader need not be reminded that turbulence is not synonymous with anomalous resistivity; in fact, it is quite difficult to make anomalous resistivity out of even the most turbulent waves.)

The effects of AC electric fields and electrostatic shock structures, together with the very important factor of ionospheric current transformation

can all be folded into a model which includes the effects of particle anisotropy and mirroring forces. The formal development is based on charge conservation (Poisson's equation, of which quasi-neutrality is a truncated form) and current conservation in the ionosphere. Chiu and Cornwall (1980) have considered such a model in dipolar magnetic geometry, coupled with ionospheric physics. In such a model the parallel potential drop is intimately coupled to the perpendicular electrostatic field structure as indicated in Figure 1.

Poisson's equation with perpendicular electric field in a dipolar magnetic field

$$\nabla\cdot\vec{E}_\perp + B\,\frac{\partial}{\partial s}\,(B^{-1}E_\parallel) = 4\pi \sum_j n_j e_j \tag{4}$$

becomes

$$K\,\nabla\cdot\vec{E}_\perp + B\,\frac{\partial}{\partial s}\,(B^{-1}E_\parallel) = 4\pi \sum_j \tilde{n}_j e_j \tag{5}$$

where K is the plasma dielectric constant:

$$K = 1 + 4\pi \sum_j \frac{\tilde{n}_j M_j c^2}{B^2} \tag{6}$$

and the density $\tilde{n}_j$ is that which would be appropriate in the absence of the perpendicular electric field. Equation (5) is an approximate generalization of Swift's formulation (1975) to an inhomogeneous magnetic field and is in agreement with Swift's own generalization (1979). The quasi-neutrality equation of Chiu and Schulz (1978) is simply that the right-hand side of (5) vanish. In fact, taking $E_\perp$ from data and $\nabla\cdot\vec{E}_\perp = E_\perp/\ell_\perp$ where $\ell_\perp$ is the perpendicular scale, one finds that the left-hand side of (5) yields a fractional charge separation $\Delta n/n = 10^{-2}$-10^{-3}. Or, looked at the other way around, this sort of charge separation can drive perpendicular electric fields of $O(M^2/\ell_\perp e)$ = 100's of mV/m, as well as parallel fields of $O[(\ell_\perp/\ell_\parallel)E_\perp]$. It should be noted that the term $B\partial(B^{-1}E_\parallel)/\partial s$ in (5) is quite negligible; it is of order $\Lambda_D^2/\ell_\parallel^2 = 10^{-8}$ where Λ_D is the Debye length. This is why ordinary double layers need such small parallel scale lengths in order for there to be appreciable charge separation. In this generalized formulation, the exis-

tence of $E_\parallel$ (independent of whether the second term on the left side of (5) is included or not) is supported self-consistently not only by particle anisotropy and mirror forces implicit in $\tilde{n}_j$ but also by the existence of perpendicular potential drops in the magnetosphere implicit in $K\,\nabla\cdot\vec{E}_\perp$, since $K \gg 1$. Thus, a discontinuity in $\nabla\cdot\vec{E}_\perp$ in the magnetosphere (Lyons, 1980; Chiu et al., 1979) an also be contributory to $E_\parallel$.

From (5), $\nabla\cdot\vec{E}_\perp$ introduces the perpendicular scale length $\ell_\perp$ of the auroral arc into the model. However, to self-consistently determine $\ell_\perp$, (5) is not enough because current and charge must also be conserved at the ionosphere. In other words, the scale $\ell_\perp$ must be such that ionospheric and magnetospheric conservation laws are both satisfied. Thus, the scale length of the perpendicular electrostatic field structure is related not only to the field-aligned current to the ionosphere but also to the ionospheric Pedersen conductivity. Thus, ionosphere-magnetosphere coupling is a crucial ingredient determining the geomatric structure as well as the energetics of the quiet auroral arc in such a model.

To incorporate ionospheric current transformation in the region (120-2000) km altitude is a very difficult task. At present, only very rudimentary methods are used to prescribe the current flow in the ionosphere and the horizontal electric-field gradients there; they are coupled by the requirement that the ionosphere must be able to balance the current flow (as well as to balance sources and sinks of charge). Two simple equations express these facts: (e.g., Atkinson, 1970; Coroniti and Kennel, 1972) the equation of current continuity

$$J_\parallel = \frac{\partial}{\partial x}\left(\Sigma_p \frac{\partial \phi}{\partial x}\right) \tag{7}$$

and of charge balance at the ionosphere

$$\frac{dN}{dt} = S - \alpha\,(N^2 - N_0^2) = 0 \tag{8}$$

In these equations, x is a horizontal north-south coordinate, Σ_p is the height-integrated Pedersen conductivity, N is the height-integrated ionospheric electron density, α is a recombination coefficient, αN_0^2 represents non-auroral sources, and S represents sources of charge from auroral electron precipitation, or from upward-going ions.

At present, no satisfactory solution of such a model has yet been obtained in the return-current region, although an approximate solution in the central electron beam region has been obtained (Chiu and Cornwall, 1980). A schematic illustration of this model is given in Figure 6. Figure 7 shows the latitudinal structure of the approximate solution which can be compared with the observed structures shown on Figure 2.

V. CONCLUSIONS AND PROSPECTS

We have undertaken a very brief review of the various mechanisms which have been invoked to account for the observed consequence of parallel potential drops in the auroral arc. Our purpose is, of course, not to address the details of these mechanisms separately but to emphasize that all the mechanisms (with perhaps the exception of Debye-length double layers) have a commonality underlying them: the unavoidable effects of particle anisotropy and mirror forces, and the necessity to include ionospheric physics as well as proper magnetospheric boundary conditions. While specific dynamical mechanisms may be of varying importance in the wide range of auroral conditions, it seems to us that particle anisotropies and mirror forces must be taken into account for most electrostatic features of the quiet arc when the parallel potential drop does not exceed a few kilovolts. For more energetic events, additional dynamical factors such as electrostatic shock and perhaps anomalous resistivity may come into play.

To formulate a unified model of arc formation, we have pointed out that the basic geometrical factors of particle anisotropy and mirror forces must be merged into the considerations of the various "mechanisms". In the light of these basic factors, consideration of the various "mechanisms" in isolation of each other has no a priori physical justification. Indeed, it is an unfortunate historical accident. Auroral physicists are now beginning to realize the necessity to unify the diverse mechanisms into a comprehensive model of auroral arc formation. The task is difficult because it must encompass both magnetospheric and ionospheric physics, but attempts in this direction are already being made (some features of these preliminary attempts are reviewed here).

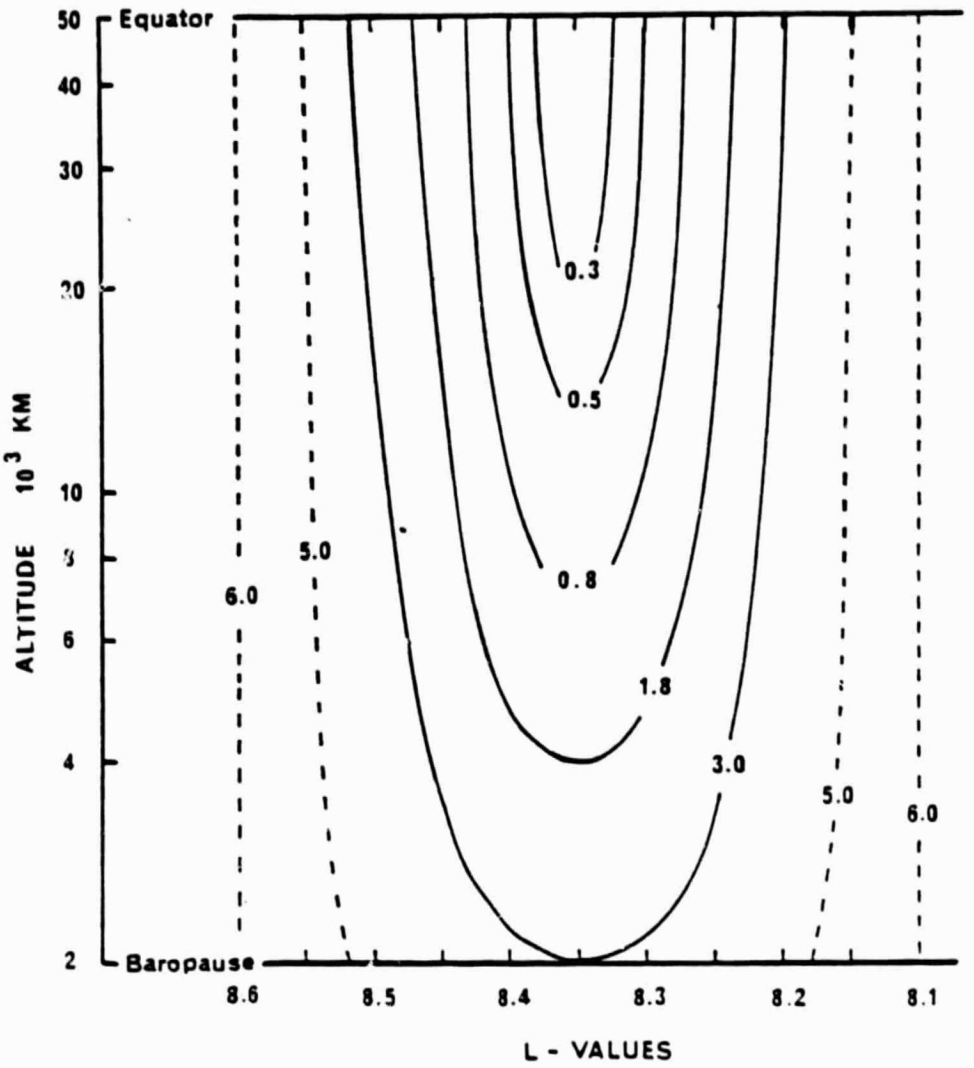

Fig. 6. Equipotential contour, in units of kilovolts, of an approximate solution of auroral electrostatic structure.

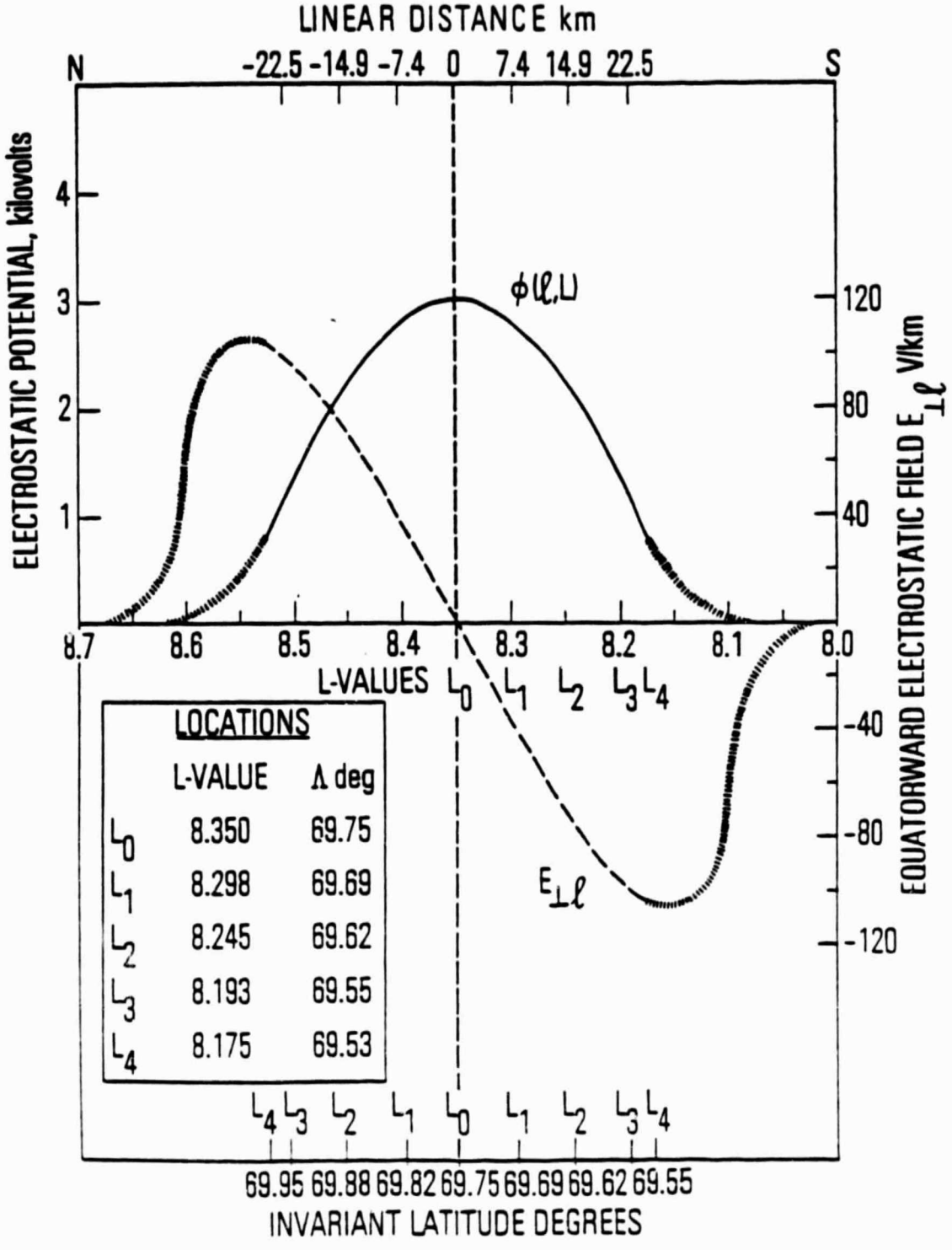

Fig. 7. Distributions of electrostatic potential U and the north-south perpendicular electrostatic field $E_\perp$ as functions of L at 2000 km altitude.

The electrodynamical structure of auroral arcs is obviously much more complex than the very simple factors distilled into the models reviewed here. The immediate prospect for these models would be to consider the basic electrodynamical structure in relation to specific phenomena one at a time. For example, the particle distribution functions in self-consistent equilibrium with the electrostatic potential ϕ need not be stable with respect to various plasma wave modes; therefore, evaluation of wave generation under the basic unavoidable conditions of particle anisotropy and mirror forces in a strong DC electric field will be an important area of auroral theory in the near future. Further, although it is outside of the scope of the present review, the effects of the plasma wave AC electric fields are bound to feed back upon the DC electric field structure and the particle distribution. The next logical step of arc-model development will probably be in this direction, thus unifying some aspects of electrostatic turbulence theory into the basic factors considered here.

REFERENCES

Alfvén, H., and C.-G. Fälthammar (1963): Cosmical Electrodynamics, pp. 163-167, Clarendon Press, Oxford.

Armstrong, J. C., and A. J. Zmuda (1973): Triaxial magnetic measurements of field-aligned currents at 800 km in the auroral region: Initial results, J. Geophys. Res., 78, 6802.

Atkinson, G. (1970): Auroral arcs: Result of interaction of a dynamic magnetosphere with the ionosphere, J. Geophys. Res., 75, 4796.

Block, L. P. (1975): Double layers, in Physics of the Hot Plasma in the Magnetosphere, pp. 229-249, edited by B. Hultqvist and L. Stenflo, Plenum Press, N.Y.

Cauffman, D. P., and D. A. Gurnett (1972): Satellite measurements of high latitude convection electric fields, Space Sci. Rev., 13, 369.

Chiu, Y. T., and J. M. Cornwall (1980): Electrostatic model of a quiet auroral arc, J. Geophys. Res., 85, 543.

Chiu, Y. T., and M. Schulz (1978): Self-consistent particle and parallel electrostatic field distributions in the magnetospheric-ionospheric auroral region, J. Geophys. Res., 83, 629.

Chiu, Y. T., J. M. Cornwall, and M. Schulz (1979): Auroral magnetosphere-ionosphere coupling: A brief topical review, Solar-Terrestrial Proceedings, ed. R. F. Donnelly, Vol. 2, p. 494, NOAA, Boulder, Colorado.

Cloutier, P. A. (1971): Ionospheric effects of Birkeland currents, Rev. Geophys. Space Phys., 9, 987.

Coroniti, F. V., and C. F. Kennel (1972): Polarization of the auroral electrojet, J. Geophys. Res., 77, 2835.

Croley, D. R., Jr., P. F. Mizera, and J. F. Fennell (1978): Signature of a parallel electric field in ion and electron distributions in velocity space, J. Geophys. Res., 83, 2701.

Evans, D. S. (1974): Precipitating electron fluxes formed by a magnetic field-aligned potential difference, J. Geophys. Res., 79, 2853.

Evans, D. S. (1975): Evidence for the low altitude acceleration of auroral particles, in Physics of the Hot Plasma in the Magnetosphere, pp. 319-340, edited by B. Hultqvist and L. Stenflo, Plenum Press, N.Y.

Frank, L. A., and K. L. Ackerson (1971): Observation of charged particle precipitation into the auroral zone, J. Geophys. Res., 76, 3612.

Fridman, M., and J. Lemaire (1980): Relationship between auroral electron fluxes and field-aligned electric potential difference, J. Geophys. Res., 85, 664.

Ghielmetti, A. G., R. G. Johnson, and E. G. Shelley (1978): The latitudinal, diurnal and diurnal and altitudinal distributions of upward flowing energetic ions of ionospheric origin, Geophys. Res. Letters, 5, 59.

Goertz, C. K. (1979): Double layers and electrostatic shocks in space, Rev. Geophys. Space Phys., 17, 418.

Heppner, J. P. (1972): Electric field variations during substorms: Ogo 6 measurements, Planet. Space Sci., 20, 1475.

Hudson, M. K., and F. S. Mozer (1978): Electrostatic shocks, double layers, and anomalous resistivity in the magnetosphere, Geophys. Res. Letters, 5, 131.

Hudson, M. K., R. L. Lysak, and F. S.Mozer (1978): Magnetic field-aligned potential drops due to electrostatic ion cyclotron turbulence, Geophys. Res. Letters, 5, 143.

Kan, J. R. (1975): Energization of auroral electrons by electrostatic shock waves, J. Geophys. Res., 80, 2089.

Kan, J. R. (1980): Comment on "Double layers and electrostatic shocks in space" by C. K. Goertz, Rev. Geophys. Space Phys., 18, 338.

Kindel, J. M., and C. F. Kennel (1971): Topside current instabilities, J. Geophys. Res., 76, 3055.

Kintner, P. M., M. C. Kelley, and F. S. Mozer (1978): Electrostatic hydrogen cyclotron waves near one earth radius altitude in the polar magnetosphere, Geophys. Res. Letters, 5, 139.

Knight, S. (1973): Parallel electric fields, Planet. Space Sci., 21, 741.

Lemaire, J., and M. Scherer (1971): Simple model for an ion-exosphere in an open magnetic field, Phys. Fluids, 14, 1683.

Lemaire, J., and M. Scherer (1974): Ionosphere-plasmasheet field-aligned currents and parallel electric fields, Planet. Space Sci., 22, 1485.

Lennartsson, W. (1977): On high-latitude convection field inhomogeneities, parallel electric fields and inverted-V precipitation events, Planet. Space Sci., 25, 89.

Lyons, L. R. (1980): Generation of large-scale regions of auroral currents, electric potentials, and precipitation by the divergence of the convection electric field, J. Geophys. Res., 85, 17.

Lyons, L. R., D. S. Evans, and R. Lundin (1979): An observed relation between magnetic field aligned electric fields and downward electron energy fluxes in the vicinity of the auroral forms, J. Geophys. Res., 84, 457.

Mizera, P. F., and J. F. Fennell (1977): Signatures of electric fields from high and low altitude particle distributions, Geophys. Res. Letters, 4, 311.

Mizera, P. F., D. R. Croley, Jr., and J. F. Fennell (1976): Electron pitch-angle distributions in an inverted-'V' structure, Geophys. Res. Letters, 3, 149.

Montgomery, D. C., and G. Joyce (1969): Shock-like solutions of the electrostatic Vlasov equation, Plasma Phys., 3, 1.

Mozer, F. S., and R. H. Manka (1971): Magnetospheric electric field properties deduced from simultaneous balloon flights, J. Geophys Res., 76, 1697.

Mozer, F. S., C. W. Carlson, M. K. Hudson, R. B. Torbert, B. Paraday, J. Yatteau, and M. C. Kelley (1977): Observations of paired electrostatic shocks in the polar magnetosphere, Phys. Rev. Letters, 38, 292.

Papadopoulos, K. (1977): A review of anomalous resistivity for the ionosphere, Rev. Geophy. Space Phys., 15, 113.

Persson, H. (1966): Electric field parallel to the magnetic field in a low density plasma, Phys. Fluids, 9, 1090.

Ponyavin, D. I., M. I. Pudovkin, and S. S. Sazhin (1977): Self-consistent field-aligned electric field in the earth's magnetosphere, Geomagnet. Aeronomy, 17, 323.

Sharp, R. D., R. G. Johnson, E. G. Shelley, and K. K. Harris (1974): Energetic O^+ ions in the magnetosphere, J. Geophys. Res., 79, 1844.

Shawhan, S. D., C. G. Fälthammar, and L. P. Block (1978): On the nature of large auroral zone electric fields at 1-R_E altitude, J. Geophys Res., 83, 1049.

Shelley, E. G., R. D. Sharp, and R. G. Johnson (1976): Satellite observations of an ionospheric acceleration mechanism, Geophys. Res. Letters, 6, 54.

Shelley, E. G., R. G. Johnson, and R. D. Sharp (1972): Satellite observation of energetic heavy ions during a geomagnetic storm, J. Geophys. Res., 77, 6104.

Swift, D. W. (1975): On the formation of auroral arcs and acceleration of auroral electrons, J. Geophys. Res., 80, 2096.

Swift, D. W. (1976): An equipotential model for auroral arcs, 2, numerical solutions, J. Geophys. Res., 81, 3935.

Swift, D. W. (1979): An equipotential model for auroral arcs: The theory of two-dimensional laminar electrostatic shocks, J. Geophys. Res., 84, 6427.

Vondrak, R. R., H. R. Anderson, and R. J. Spiger (1971): Rocket-based measurements of particle fluxes and currents in an auroral arc, J. Geophys. Res., 76, 7701.

Whipple, E. C., Jr. (1977): The signature of parallel electric fields in a collisionless plasma, J. Geophys. Res., 82, 1525.

Exhibit B: On the Structures of Auroral Acceleration Potentials, by Y. T. Chiu, A. L. Newman and J. M. Cornwall

On the Structures of Auroral Acceleration Potentials

Y. T. Chiu and A. L. Newman
Space Sciences Laboratory
The Aerospace Corporation
El Segundo, California 90245

J. M. Cornwall
Department of Physics
University of California at Los Angeles
Los Angeles, California

January 1981

This work is supported in part by NASA Headquarters Contract NASW-3327 and in part by NASA Solar-Terrestrial Theory Program Contract NASW-3434.

Abstract

We examine the self-consistency of magnetospheric and ionospheric boundary conditions of a kinetic model of magnetospheric-ionospheric electrodynamical coupling in the aurora formulated by Chiu and Cornwall (1980). This model includes the kinetic current conservation model of Lyons (1980); but in addition, it demands self-consistency between kinetic charge distributions and the divergence of the electric field in accordance with Poisson's equation. It is found that the structures of the ionospheric electric potential in response to imposed magnetospheric structure takes a variety of shapes in agreement with the "V-shaped" and "S-shaped" structures measured by electric field measurements on board the S3-3 satellite. In the absence of a parallel potential drop, the "mapping" of electric fields from the magnetosphere to the ionosphere is strictly dictated by the geometry of the magnetic field. With the presence of a kinetic model parallel potential drop, the "mapping" of electric fields between the magnetosphere and ionosphere is formulated here in terms of our Green's function treatment. It is shown that the new "mapping" filters out structure scales larger than an inverted-V scale (50-150 km) determined by the ionospheric Pedersen conductivity. All structure scales smaller than this natural scale can be "mapped through" from the magnetosphere to the ionosphere.

Exhibit C: Sferics in the Stratosphere, by R. H. Holzworth and Y. T. Chiu

SFERICS IN THE STRATOSPHERE

by

Robert H. Holzworth and Yam T. Chiu
Space Sciences Laboratory

THE AEROSPACE CORPORATION
El Segundo, California 90245

APRIL 1980

This article will appear as Chapter 16
in Handbook of Atmospherics by CRC Press.

This work was supported in part by NASA Contract NASW-3327.

I. INTRODUCTION

Unlike sferics in the lower troposphere, a sferic seen from the stratosphere is not usually characterized by an ionization channel produced by a visible electrical discharge. The ambient conductivity above 20 km altitude is generally sufficient to carry a sferic related current pulse without electrical breakdown. This is a result both of the higher ambient electrical conductivity as well as the larger area available for a current path as the signal propagates further away from the source in the cloud. To date very few in situ measurements of sferic-related electric currents and fields in the stratosphere have been reported.

Sferic electrical measurements made onboard aircraft flying over thunderstorms in the troposphere have a long history (cf. Wait, 1953; Stergis et al., 1957; and Vonnegut et al., 1966). More recently, stratospheric sferics have been detected with high-altitude-balloon-borne electrical instrumentation by Benbrook et al. (1974), Burke (1975) and Holzworth (1980).

These three recent works have concentrated on thunderstorm related stratospheric electric fields in general and each reported briefly on stratospheric sferic signatures. This chapter will extend these and the earlier works by describing stratospheric sferic related electric field detection methods and present observations of a variety of different signatures. Propagation of the sferic source disturbance in the stratosphere from which a physical description of the observed time scale and signatures can be determined, will be mathematically described.

II. STRATOSPHERIC ELECTRIC FIELD INSTRUMENTATION

The detector used in the experiments described below is a double Langmuir probe specifically designed to operate in the stratosphere (see Figure 1). The device measures the potential difference between two identical, separated conductors with a differential operational amplifier. The electric field component along the line between the two probes is the potential difference divided by the probe separation distance.

Many theoretical and experimental discussions of the double Langmuir probe (see Mozer, 1973, and references therein) have shown its applicability to balloon-borne measurements the absolute dc electric field in the stratosphere to an accuracy of a few millivolts/meter. This section will discuss the particular problems encountered when applying the double-probe technique to the upper atmosphere and describe the physical apparatus used in the experiments.

The presence of small molecular ions provides the atmosphere with a low electrical conductivity ranging on the average from 5×10^{-13} mho/m at the ground to 10^{-11} mho/m at 30 km altitude. In order to make a double-probe potential difference measurement in the atmosphere the detector must have an effective internal electrical resistance which is extremely high for the following reason. The potential difference V in the atmosphere will cause a current V/R_{in} to flow through the electronic input impedance R_{in}. This current returns through the atmosphere along a path with resistance R_{atm}. R_{atm} is computed from the required potential difference to collect a given current where that current is impeded by the atmospheric resistivity. Mozer and

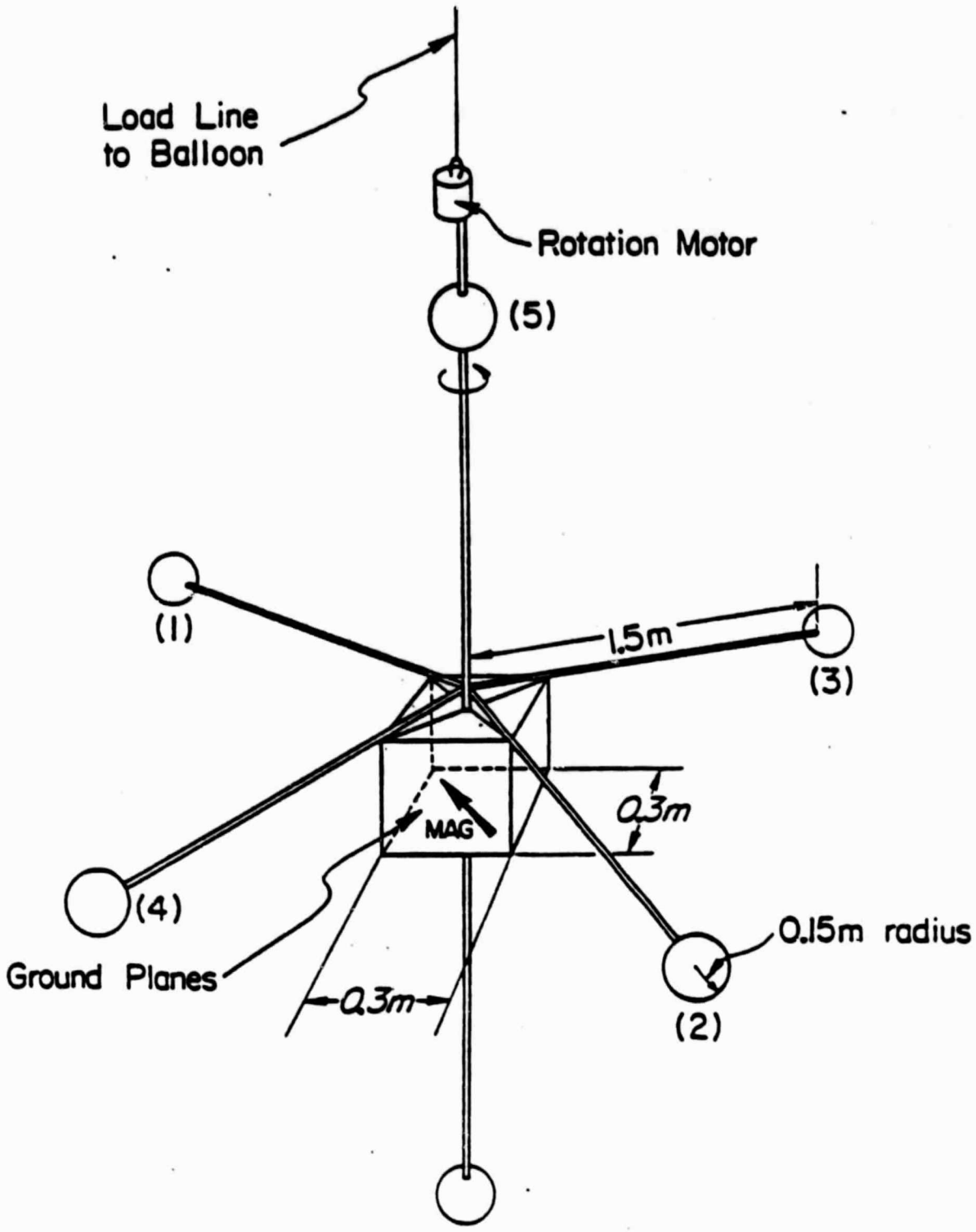

Figure 1. Stratospheric electric field detector showing three pairs of mutually orthogonal spherical probes. Numbers on probes are referenced in later figures.

Serlin (1969) calculate that for a spherical probe of radius r_o in the atmosphere with conductivity σ, that $R_{atm} = \frac{1}{4\pi r_o \sigma} = 10^{11}\Omega$ at 30 km altitude. Unless $R_{in} >> R_{atm}$ the voltage divider effect of these two resistors will cause most of the voltage to appear across R_{atm}. Thus to measure an unattenuated value of V the electronics must satisfy $R_{in} >> R_{atm}$. For the detector to meet the requirement of high internal impedance ($Z > 10^{14}$ ohms), the input signal from each separated conductor is fed into a very high impedance FET operational amplifier (op amp). In addition to this op amp at the input, the complete instrument is designed in a manner so as to reduce leakage currents. Reducing the leakage is accomplished by circuit design considerations as well as external electrical cleanliness. The shield of the coaxial cable to the probe is driven at the same potential as the probe itself, thereby reducing leakage. Driving the shield at the probe potential also eliminates capacitive currents which might derive from physical motions of the instrument. The op amps themselves are mounted on a high impedance teflon base and then electrically shielded. The external surfaces of the instrument that are in contact with the probes must also have high electrical resistance. The fiberglass booms on which the probes are mounted are carefully cleaned with Freon and dried in a clean environment to remove all oils and moisture both inside and out. A high impedance coaxial cable is then cleaned and strung down the center of the boom and both ends are plugged.

Two of the difficulties encountered when making a potential difference measurement in the atmosphere arise from work function differences between the two probes and from photoelectric emission currents to the probes. The work function differences are minimized by two processes. The probes are entirely coated with a solution of aqueous carbon called "aquadag" which helps to make the work function uniform. During data collection the entire apparatus is

rotated about a vertical axis. The difference in potential between the two probes due to an external electric field will then appear as a sinusoidal voltage variation in the difference measurement, but any remaining net work function difference between the probes will then be measurable as a dc offset of this sinusoidal voltage. Therefore, analyzing just the oscillatory part of the output signal allows efficient removal of these work function errors in the horizontal electric field measurement and determines the real zero voltage base line for transient events.

The photoelectric effect can cause a significant current to the probe if the flux of ultraviolet (UV) radiation is large. At balloon float altitudes near 20 kilometers the photo current is not significant because most of the UV absorbing ozone is above this altitude. However, for experiments above 30 to 35 kilometers the photoelectric current can be significant for several hours on either side of the diurnal maximum zenith angle. To minimize this problem, probes for high altitude experiments are designed to have equal solar cross-section and are usually spherical so that the photoelectric current is nearly the same for both probes. Thus the net current to the probes from this effect will produce only a small dc offset.

The probes along the spin axis must make an absolute potential difference measurement without the benefit of the regular payload rotation. Thus the vertical potential difference measurement will be biased by work function offsets. This dc offset in the vertical electric field measurement can amount to about a ±20 mV/m uncertainty in the vertical electric field, which is small compared to the atmospheric electric field at 30 km altitude and small compared to most sferic fields. Because of this inherent vertical field uncertainty and because this bulky balloon payload is difficult to launch, it is sometimes desirable to remove the lower vertical boom. Then the vertical

electric field is determined from the potential difference between the upper probe and the average of the four horizontal probes. This makes the signal to noise ratio lower by a factor of 2 and the probes slightly asymmetric, but the lack of a lower boom makes the awkward payload in Figure 1 considerably easier to launch. The data presented in this chapter are from payloads without the lower vertical probe. The instruments flown were composed of five conductors, either one-foot square flat plates or spheres each a foot in diameter on three mutually orthogonal pairs of booms surrounding a conducting payload ground. Whether spheres or the less expensive flat plates are flown depends on the magnitude of the expected photoelectric current at the balloon float altitude. Above the uppermost vertical sphere is a small motor which is connected to the load line and provides the fifteen second rotation period. The entire payload, including telemetry electronics, altimeter, aspect magnetometer, and power supply, weighs about 30 pounds.

The potential differences between the three orthogonal sets of double probes are telemetered to a ground receiving station by various methods. The current payload configuration employs an onboard analog to digital converter from which the subsequent biphase encoded PCM modulation signal makes downstream data processing simple and accurate.

III. OBSERVATIONS OF SFERICS OVER THUNDERSTORMS

Much has been written about the quasi-dc fair weather electric field in the stratosphere (cf. Mozer and Serlin, 1969; Mozer and Lucht, 1974; Holzworth et al., 1977). However, very few observations of thunderstorm related stratospheric electric fields have been reported. This section will summarize the electric signatures of sferics as seen in hundreds of hours of balloon data collected near 30 km altitude by R. Holzworth and F. Mozer at the University of California, Berkeley.

Figure 2 shows the time history of a large thunderstorm in the dc electric field at 27 km. This data was taken in August 1974 from a balloon flight out of Ft. Simpson, N.W.T., Canada. The coordinate system used for all figures in this chapter has x in the eastward magnetic direction, y in the northward magnetic direction and z in the vertically upward direction. Thus a fair weather vertical field would point toward the ground and would be negative. The upper panel in Figure 2 is the vertical field which shows ambient fair weather electrical conditions of a few hundred mv/m negative both prior to and following the thunderstorm. During the storm there appear to be two cells or two fronts passing under the balloon with the second larger than the first. The total horizontal electric field is shown in the central panel for completeness and the bottom panel shows the sferic rate. For more detailed discussion of the dc effects on all three electric field components and the conductivity during such a thunderstorm, the reader is referred to Holzworth (1980). In the time history of the sferic rate one can again see the double peaked structure although the peaks do not coincide in time. This figure is to be used as a description of the ambient conditions during which detailed individual sferics will be analyzed below.

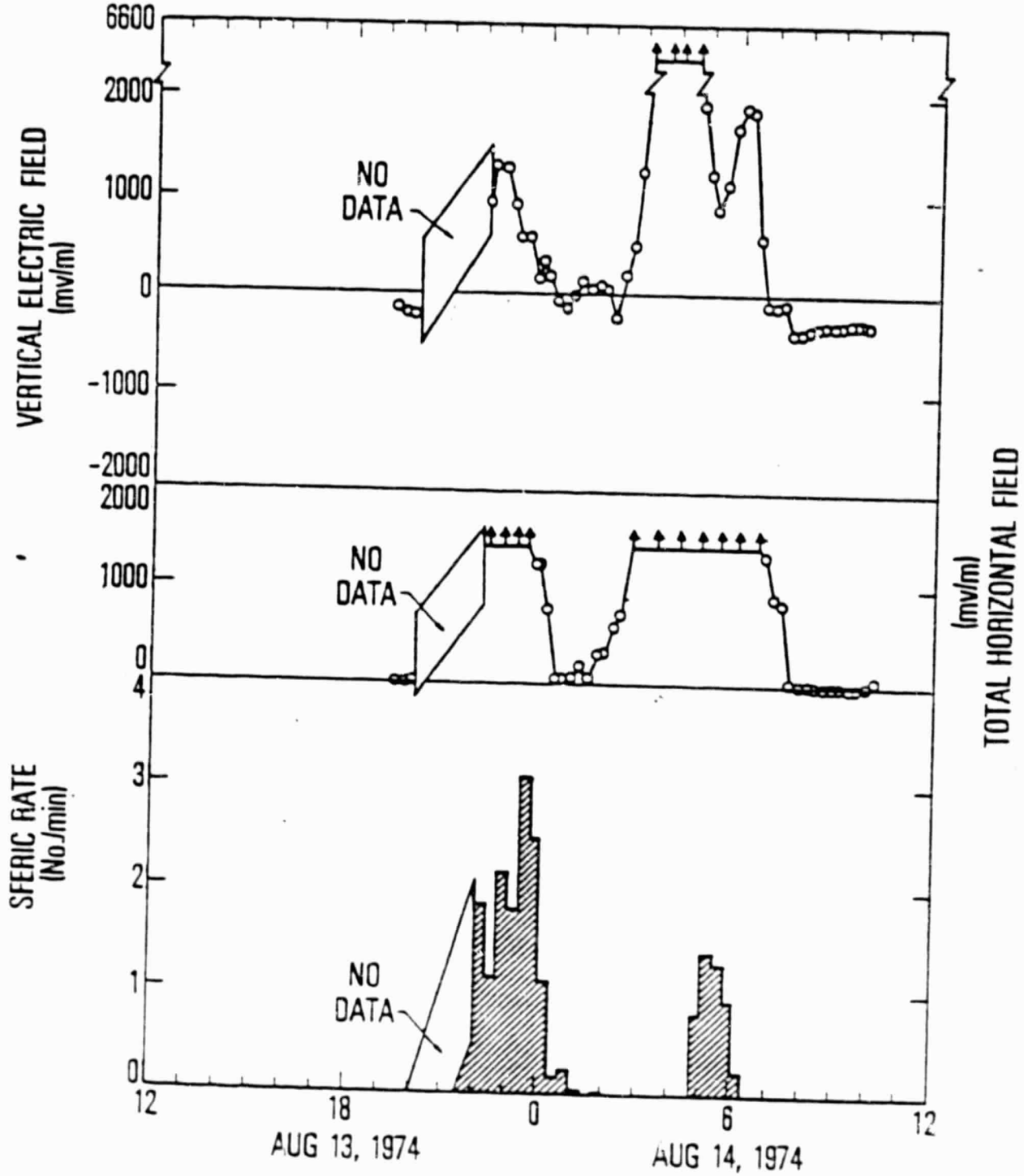

Figure 2. DC electric field over a large thunderstorm near Fort Simpson, N.W.T., Canada (62° N, 121.5° W). The upper panel is the vertical electric field, central panel is the absolute value of the total horizontal electric field ($\sqrt{E_x^2 + E_y^2}$) and the bottom panel is the sferic rate.

Figure 3 is also for background purposes and shows two DMSP weather photographs at times which bracket the data in Figure 2. No other observational weather data is available other than detailed launch site reports of the local cloud formations and precipitation. The balloon moved at about 15 knots so the weather at the local launch site was not directly applicable to that under the balloon by a few hours after launch. In any event the most that can be said is that an extensive cloud system did sweep from northwest to southeast across the region as shown in Figure 3 and that sferics were reported on our radio telemetry frequencies as well as ground reports of visible lightning and thunder throughout much of the flight.

Figure 4 shows a 20-minute segment of electric field data during the thunderstorm of Figures 2 and 3. The large spurious signals are directly correlated to static noise bursts over the audio frequency telemetry channel and correspond to sferics. The top panel of Figure 4 is the vertical electric field at lowest gain while the second panel from the top is also the vertical field but now at a gain up by 5. The bottom two panels each show the potential difference between one of two opposite horizontal probes to payload ground. V4 is 180 degrees away from V3. Due to various gain channels available the horizontal antennas were often saturated while the lowest gain vertical was never saturated in this figure.

The data from the horizontal probes (V_3 and V_4 in the bottom two panels) represent the individual probe voltages relative to payload ground. They have been presented individually in order to show the dramatic effect on payload ground as the sferic passes. Careful inspection of these figures will show that outside of the sferic transients, V_4 and V_3 always have the opposite sign at any given time. In the case of every sferic in Figure 4, the signals from the two opposite horizontal probes depart from the baseline in opposite direc-

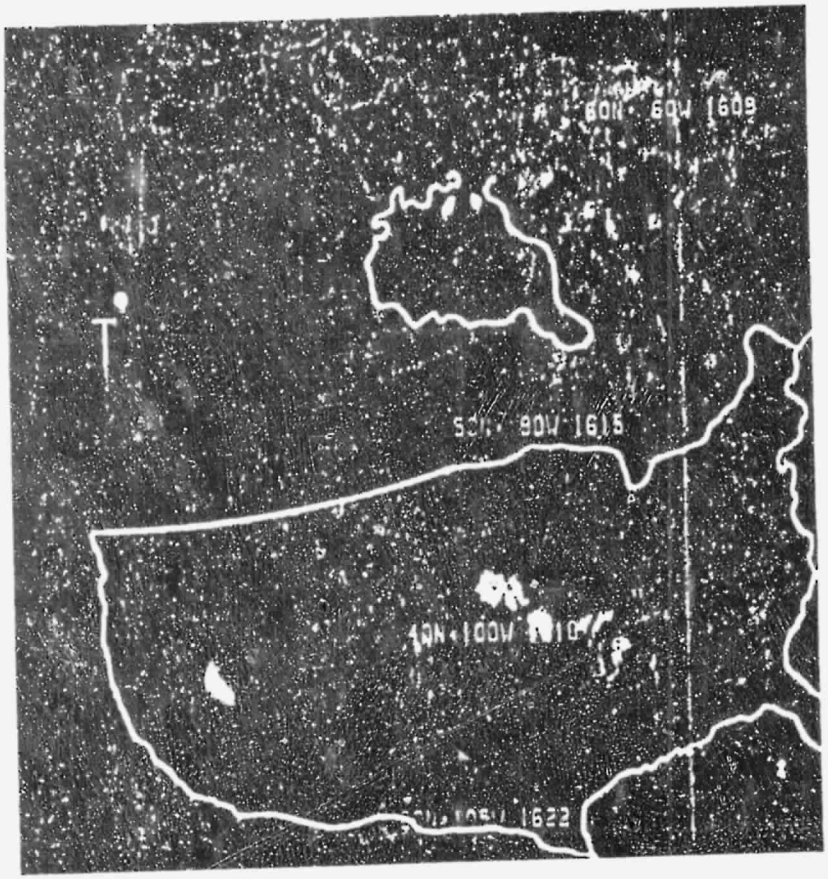

8/13/74 1601 UT

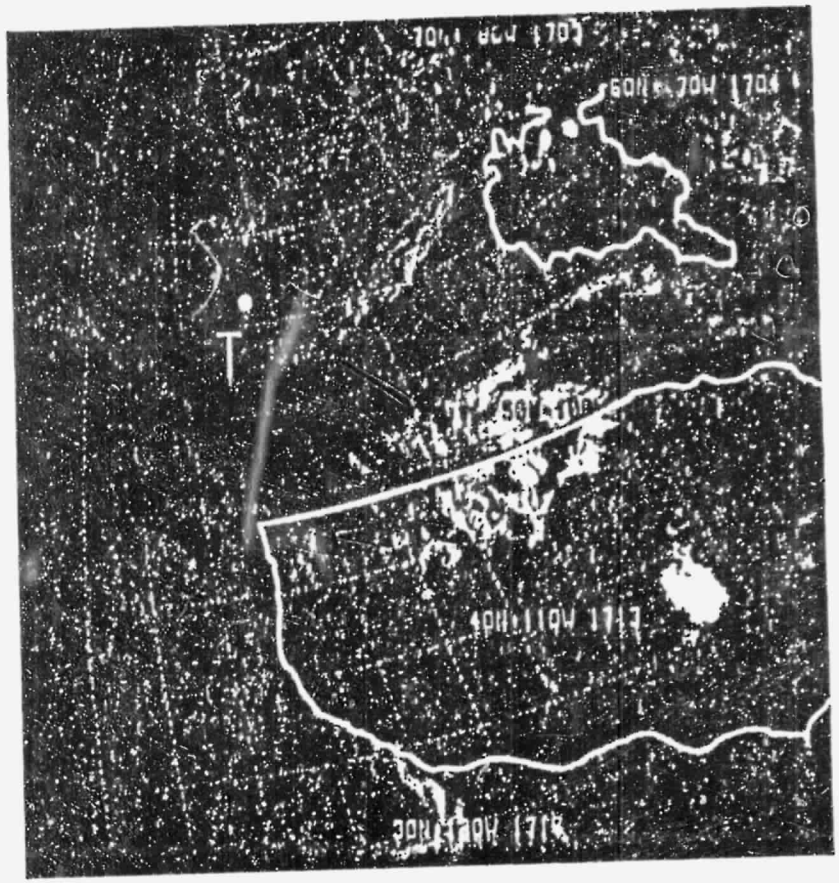

8/14/74 1656 UT

Figure 3. Two DMSP weather photos bracketing the data in Figure 2. The telemetry site at Fort Simpson is indicated with a T. This pair of photos, which are about a day apart, indicate that a heavy cloud cover passed over the area of the balloon sometime between the times of the pictures.

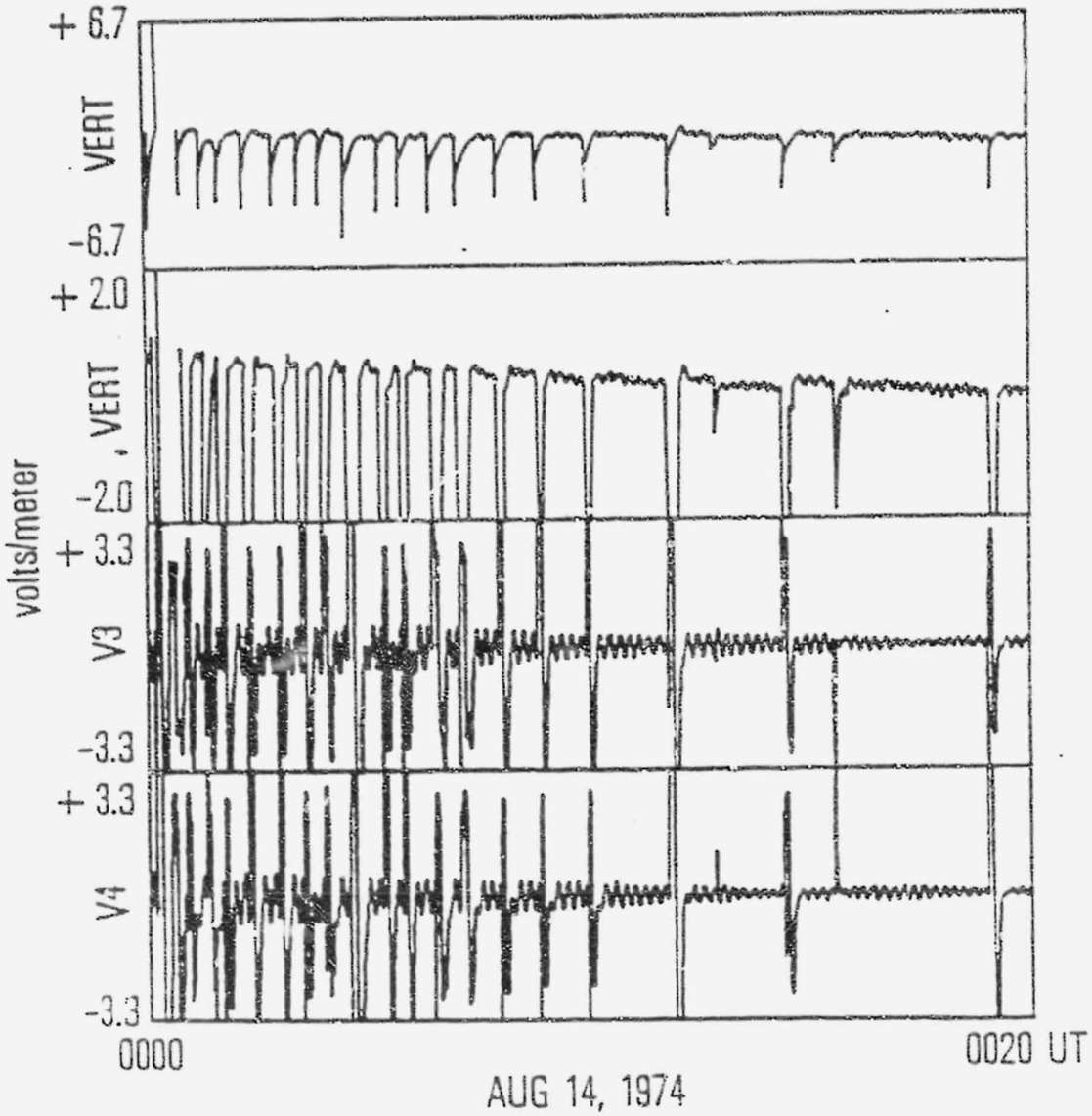

Figure 4. Twenty minutes of raw electric field data during the thunderstorm of Figures 2 and 3. The two upper panels are the vertical electric field, E_z, at two different gains. The bottom two panels are two measurements of the horizontal electric field from probes 3 and 4 which are 180° out of phase. (See Figure 1 for orientation.) The background oscillatory electric field of the bottom two figures is due to the ambient DC electric field while the spikes are due to sferics.

tions initially. Then, however, the payload ground goes alternately very high then very low as seen when V_4 and V_3 have the same sense near the end of each large sferic. This payload ground fluctuation has been removed from the upper two vertical panels showing the horizontal field by subtracting the average of all four horizontal probe signals from the upper vertical probe potential. This payload ground transient is seen consistently throughout our data set for all large sferics but does not affect our high impedance circuitry which is highly current protected. There are at least two smaller sferics in Figure 4 which were unaccompanied by ground transients and several others in later figures. The next to the last sferic in Figure 4 at about 0016 UT which did not cause a ground fluctuation will be evaluated more carefully later.

There are many features to note from this figure. First of all, most sferics last for about 5 to 10 seconds and have the sense which would appear from the rapid ramoval of positive charge below followed by the slower return to prestroke values. Another interesting thing to note in Figure 4 is that the sferics are not always related to major changes in the dc level. This can only be accurately determined for dc steps larger than about 100 mv/m from these data because of the residual rotation period fluctuation in the vertical data due to slight asymmetries of the verical measurement probes. However, small discrete dc steps are sometimes seen as shown below.

The next three figures show other 20-minute sequences of data containing sferics. Figure 5 is from the same thunderstorm shown in Figures 2-4 and shows an epoch between the two major activity periods of the storm. The interesting feature is the sferic near 0056 UT which has a positive precursor to the negative sferic transient. This brings up the point of temporal resolution. All of the data in this chapter were telemetered at a rate allowing complete vector field determination every 0.5 second. Thus, while the elec-

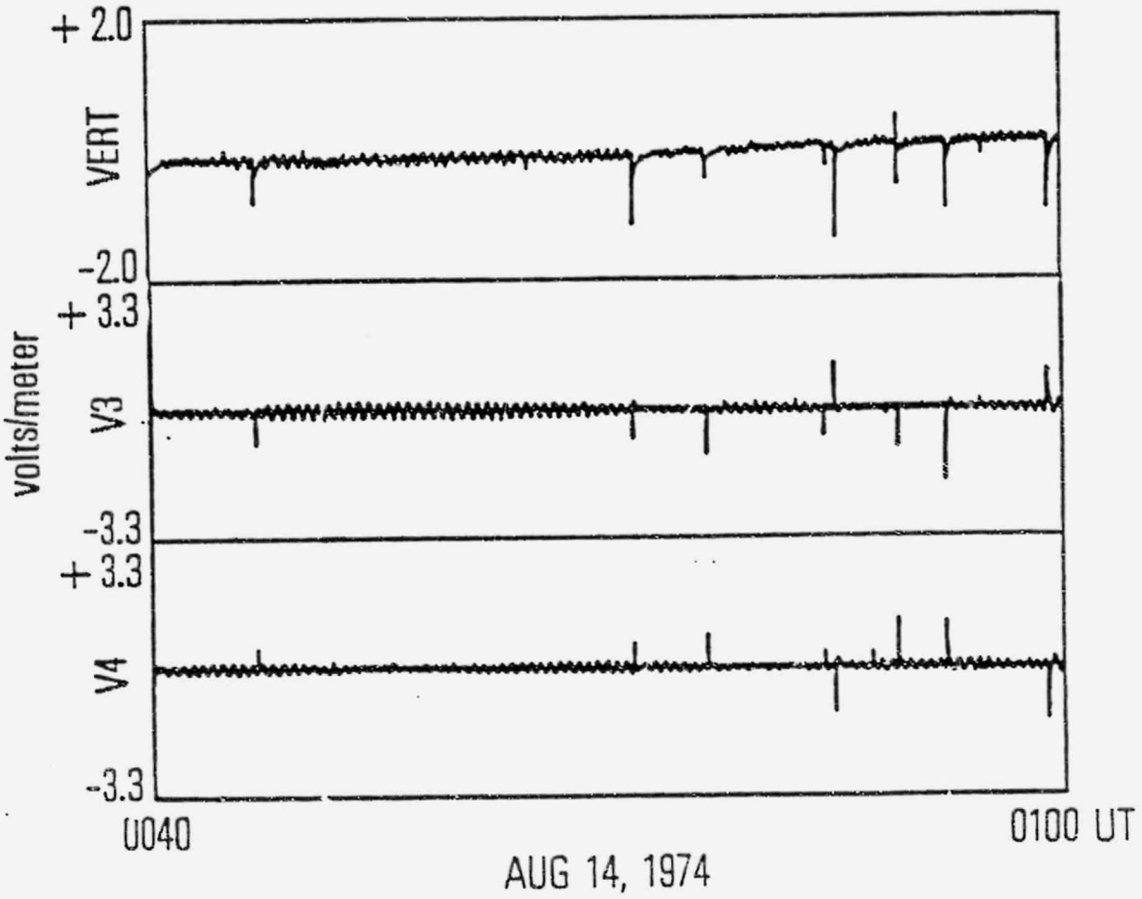

Figure 5. Twenty minutes of raw electric field data from a later time of the same thunderstorm as Figure 4. Note: the positive precursor in the sferic at 0057 UT in the vertical field.

tronics are much faster than this, time resolution is limited by the telemetry. It is therefore possible that more of the sferics displayed in this chapter actually had positive precursors but were missed because of time resolution. This type of precursor will be seen again in a later figure.

Figures 6 and 7 show two succeeding 20-minute segments of data during a thunderstorm seen from a flight over Thompson, Manitoba, Canada in August 1978. In this flight, as before, there is only a single upper vertical probe from which the average of the horizontal probes is subtracted. However, now the horizontal field is very large making the asymmetries between the payload ground planes and the upper vertical probe more apparent. The difference between V_4 and V_3 in the lower panels (or just the envelope of their signals) divided by probe separation gives the horizontal fields. In this case a horizontal potential difference of up to 8.0 volts (in Figure 6) divided by probe separation gives a horizontal field of over 2.5 volts/meter. This is over twice as large as the vertical field seen in the upper panel. Also, in this figure it is now possible to see a net dc shift of about 300 to 400 mv/m in the vertical field after a sferic at 2302.5 UT. The next 20-minute period in Figure 7 shows a lessening in severity of the storm and a gradual return to lower vertical and horizontal dc fields. The last two sferics in Figure 7 are quite interesting in that two have an inverted polarity. The last one again shows a precursor but now in the negative sense compared to that in Figure 5.

A summary of the sferic signatures seen in the vertical field on these balloon flights is shown in Figure 8. Of the four basic signatures the most common in all these data is the top one of Figure 8, namely, that which would be expected by the removal of positive charge below. The other three cases are seen only rarely with Figure 7 showing the only example we have seen of an inverted polarity stroke with an opposing precursor as in the bottom signature

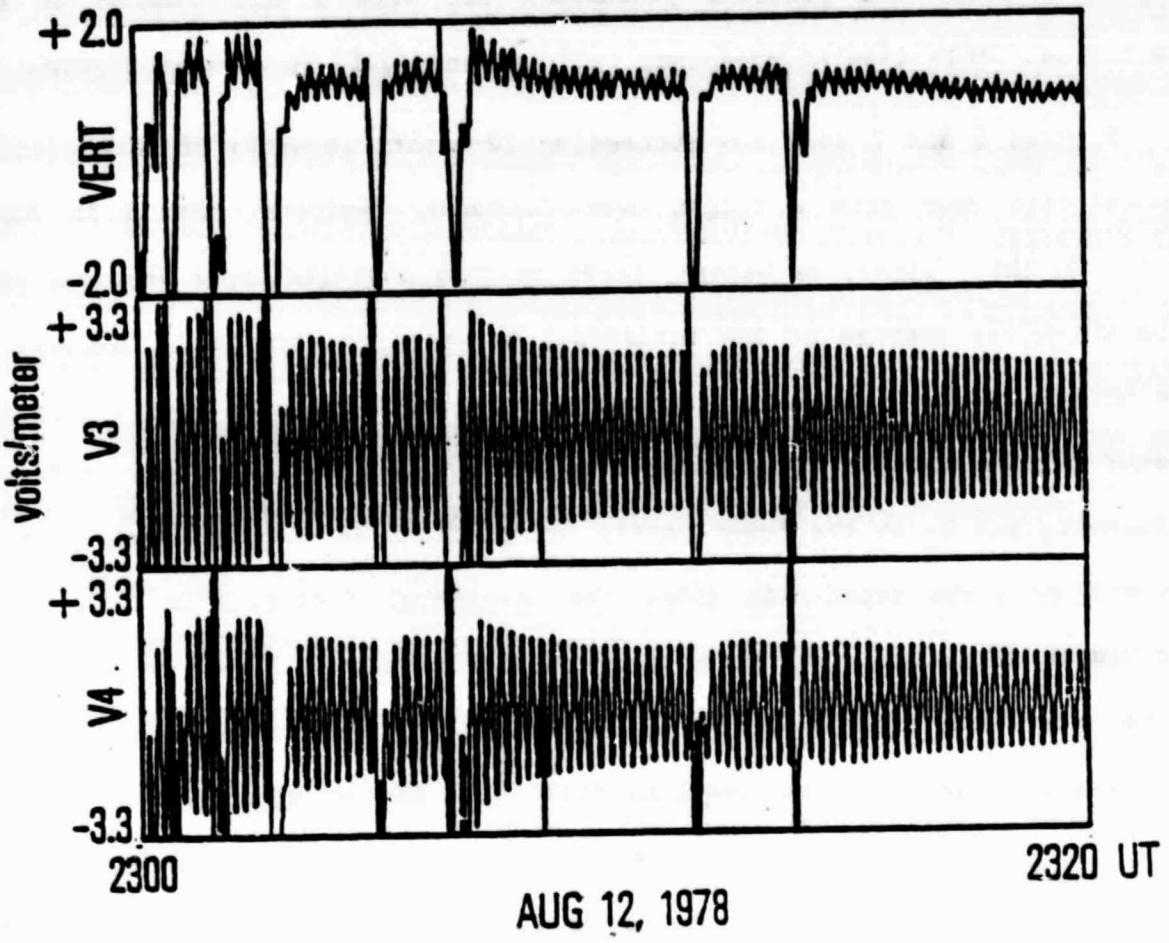

Figure 6. Twenty minutes of raw electric field data during a balloon flight from Thompson, Manitoba, Canada (55° 45'N, 97° 51'W). DC shifts resulting from the sferics are now visible in the vertical field. In this case the ambient horizontal electric field is larger than the vertical field.

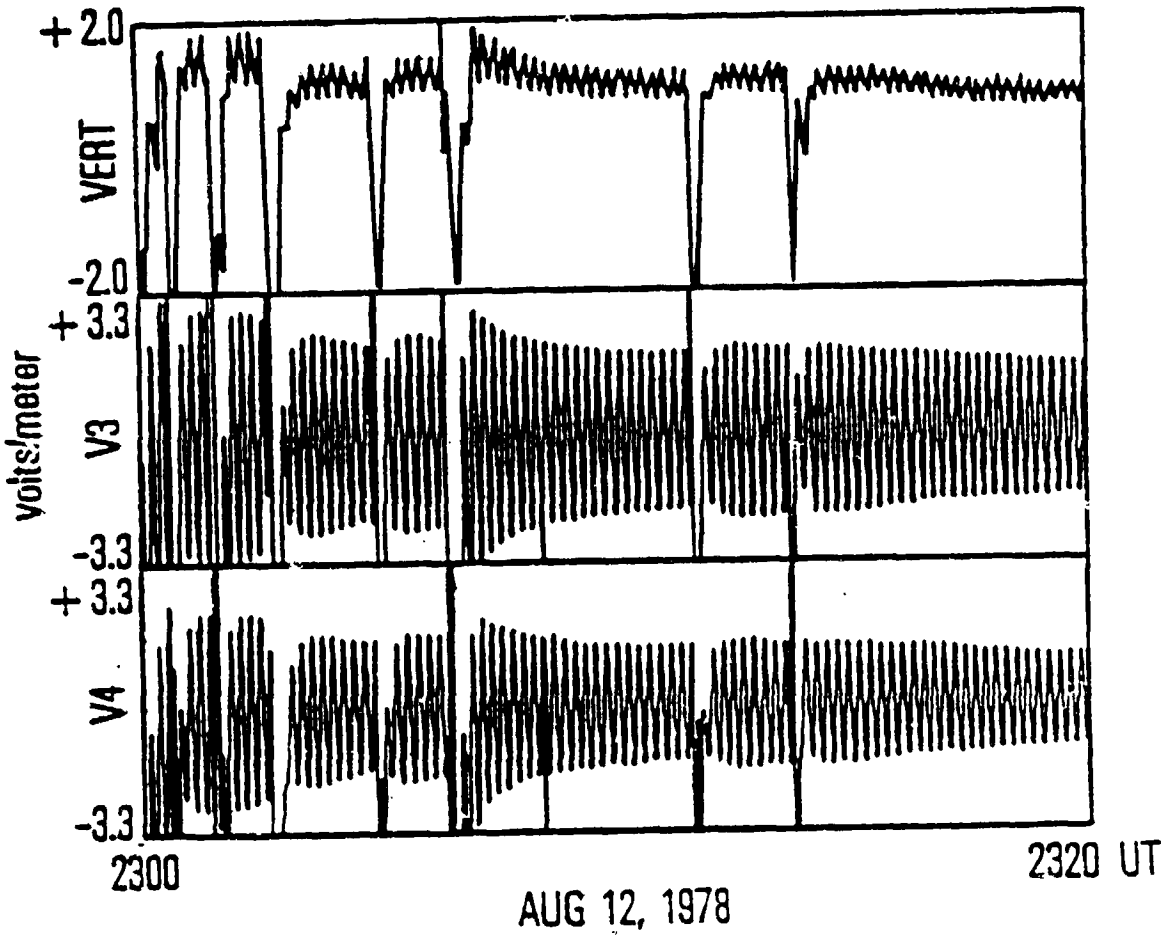

Figure 6. Twenty minutes of raw electric field data during a balloon flight from Thompson, Manitoba, Canada (55° 45'N, 97° 51'W). DC shifts resulting from the sferics are now visible in the vertical field. In this case the ambient horizontal electric field is larger than the vertical field.

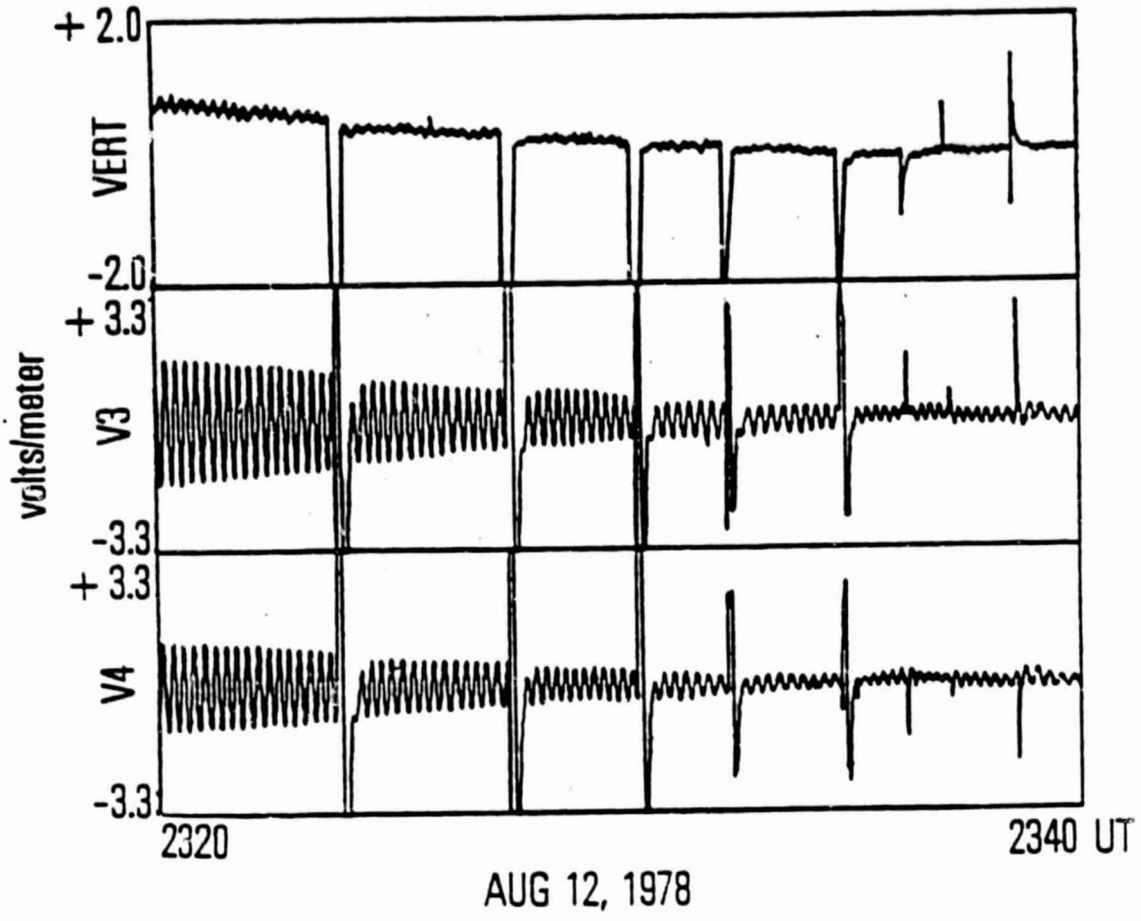

Figure 7. Twenty minutes of raw electric field directly following data in Figure 6. Note: the reversed sferic orientation and precursor near the right hand end of the vertical field panel.

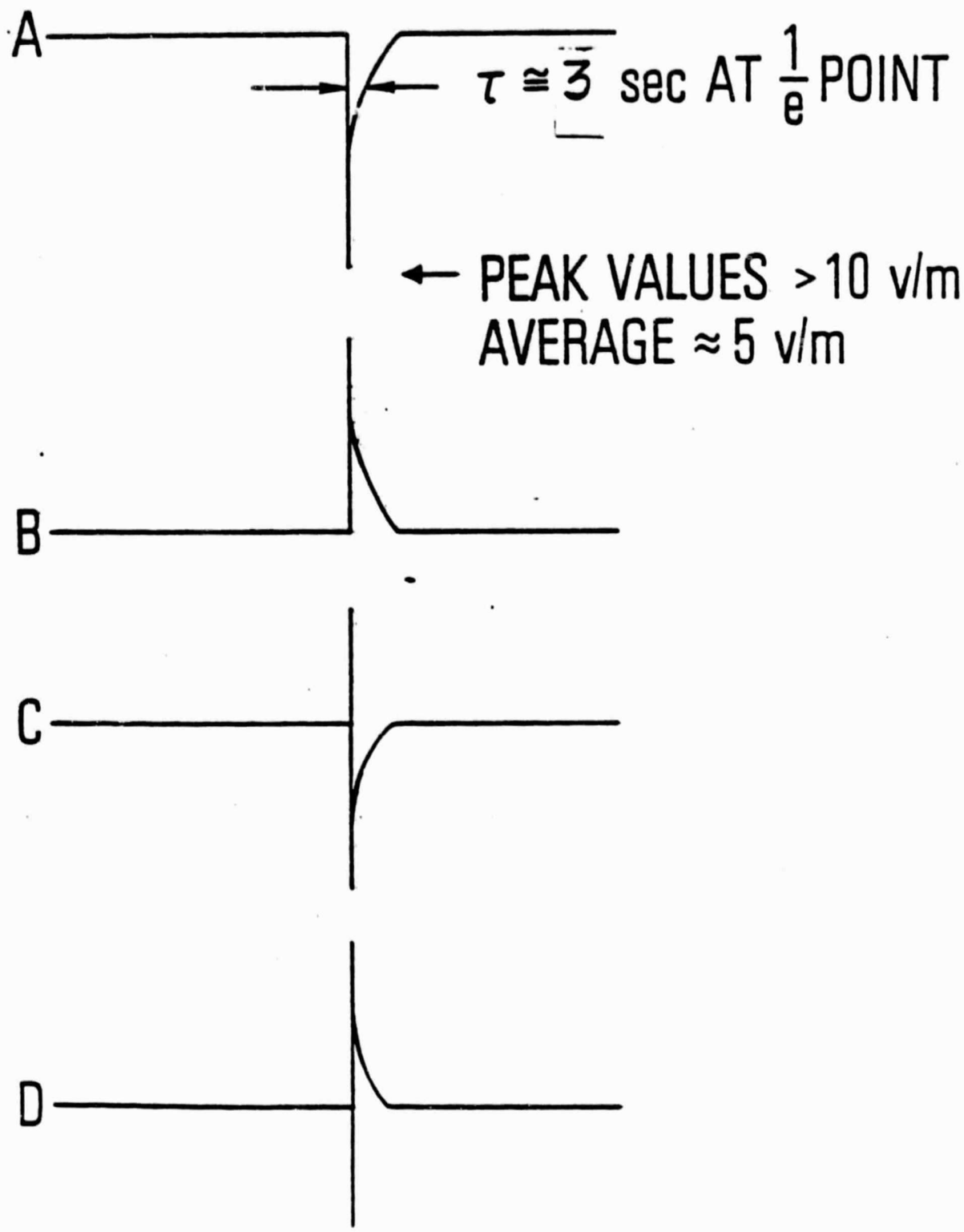

Figure 8. Schematic summary of the sferic signatures seen in the raw electric field at stratospheric altitudes.

of Figure 8. Figure 8 also summarizes the average decay time constant of these sferics which is about 3 seconds at the 30 km altitude level.

IV. THEORY OF SFERIC PROPAGATION IN THE STRATOSPHERE

In order to interpret the sferic signal structures detected by electric field measurements in the stratosphere, it is not only necessary to have firm information on the spatial and temporal structures of lightning discharge currents, but it is also necessary to establish basic ideas about sferic propagation. The necessity to unravel these two factors in data interpretation is simply that time scales of the sources are folded into time scales of the propagation medium to produce the detected signal. While the characteristics of lightning discharge currents are dealt with in Chapter 2, the theory of sferic propagation in the stratosphere will be reviewed and formulated in such a way that the relationship between source, propagation medium and detected signal will become transparent. This entails extensive usage of the theory of Green's functions.

The theory of sferic propagation in the stratosphere, over horizontal distances which are short compared to the Earth radius, is simply the theory of electromagnetic wave propagation in a horizontally stratified conducting medium, whose conductivity is a scalar. Obviously, this statement applies only to the signals propagating directly from the source into the stratosphere; the subjects of ionospheric reflection, Schumann resonances and tensor conductivity in the upper atmosphere are outside of the scope of this chapter, the primary purpose of which is to discuss the stratospheric sferic signal structure of the longest time scales (> 1 sec). Even so, the general electromagnetic character of the theory of sferic propagation in the stratosphere is not widely appreciated. This is due primarily to the traditional development of the theory, emerging from the Green's function theory of the electrostatic signature of charge-separated cloud structures (Holzer and Saxon, 1952) to

considerations of time-dependent electric signatures of the cloud structures (Anderson and Freier, 1969; Illingworth, 1972). These studies, some recognizing the significance of the Green's function approach, justifiably simplified the theory by exploiting the condition of current conservation and by ignoring Faraday's law of induction to eliminate the magnetic field. Such theories are not sferic theories in the proper sense because the signal, not being an electromagnetic wave, is not radiated. With the advent of measuring ionospheric potential differences at balloon altitudes (Mozer and Serlin, 1969, Mozer, 1971a and 1971b), interests in the transmittal of ionospheric or tropospheric potential differences through the upper atmosphere were enhanced in the early parts of the past decade (Reid, 1965; Kellogg and Weed, 1969; Atkinson et al., 1971; Volland, 1972; Park and Dejnakarintra, 1973; Bostrom and Fahleson, 1974; Chiu, 1974). These studies, some involving the detailed conductivity structure of the upper atmosphere, are primarily concerned with the transmission of sinusoidal spatial and/or temporal fields of given scale; therefore, only limited interpretation on the source and stratospheric signal structure of sferics can be obtained from these studies. Nevertheless, the enhanced interest stimulated more considerations of sinusoidal structures (Dejnakarintra and Park, 1974; Bostrom and Fableson, 1974) in which the importance of the electromagnetic character of sferics at altitudes below ~ 70 km was recognized. Therefore, it remains for us to bring this development to its next logical step, which is to provide the formal and semi-quantitative mechanism for the link between source structures and the structures of stratospheric sferic signals.

Since our problem, as defined above, concerns the radiation of the sferic signal in a conducting medium, sources are an integral element in the formulation in terms of Maxwell's equations. We assume the stratospheric medium to

be nonpolarizable and nonmagnetizable, to have the permitivity and permeability of free space, and to have a horizontally stratified scalar conductivity $\sigma(z)$. Electric and magnetic fields ($\vec{E}$, $\vec{B}$) arise as the result of a distribution of source charges Q_s ($\vec{r}$, t) and source currents $\vec{J}_s$ ($\vec{r}$, t). These fields and sources are governed by Maxwell's equations:

Gauss' laws:
$$\epsilon_o \nabla \cdot \vec{E} = Q_s \tag{1}$$

$$\nabla \cdot \vec{B} = 0 \tag{2}$$

Faraday's law:
$$\nabla \times \vec{E} + \frac{\partial \vec{B}}{\partial t} = 0 \tag{3}$$

Ampere's Law:
$$\frac{1}{\mu_o} \nabla \times \vec{B} = \sigma \vec{E} + \vec{J}_s + \epsilon_o \frac{\partial \vec{E}}{\partial t} \tag{4}$$

In (4), $\sigma\vec{E}$ is the conduction current in the stratosphere associated with the radiated field $\vec{E}$. From these Maxwell's equations, one derives the coupled radiation field equations in terms of a vector potential $\vec{A}$ and a scalar potential ϕ such that

$$\vec{B} = \nabla \times \vec{A} \tag{5}$$

$$\vec{E} = -\nabla\phi - \frac{\partial \vec{A}}{\partial t} \tag{6}$$

The potentials are governed by the coupled inhomogeneous equations

$$-\nabla^2\phi - \frac{\partial}{\partial t}(\nabla \cdot \vec{A}) = \frac{1}{\epsilon_o} Q_s \tag{7}$$

$$-\frac{1}{\mu_o}\nabla^2\vec{A} + \frac{1}{\mu_o}\nabla(\nabla\cdot\vec{A}) = -\sigma\nabla\Phi - \sigma\frac{\partial\vec{A}}{\partial t} + \vec{J}_s - \varepsilon_o\frac{\partial^2\vec{A}}{\partial t^2} - \varepsilon_o\frac{\partial}{\partial t}(\nabla\Phi) \quad . \quad (8)$$

These equations have the disadvantage of being intractable even if a convenient gauge for $\vec{A}$ is chosen. Indeed, (7) and (8), when solved, would yield much more information than the currently available stratospheric sferic data, since only sferic electric field measurements are available. Thus, we use an exact but slightly different reduction of Maxwell's equations (1) - (4) to obtain a single vector equation for the electric field. By taking the time derivative of (4) and subsequent use of (1) and (3) to eliminate the magnetic field, we arrive at the stratospheric sferic equation

$$\nabla^2\vec{E} - \frac{1}{c^2}\frac{\partial^2\vec{E}}{\partial t^2} - \mu_o\,\sigma(z)\,\frac{\partial\vec{E}}{\partial t} = \mu_o\frac{\partial\vec{J}_s}{\partial t} + \frac{1}{\varepsilon_o}\nabla Q_s \qquad (9)$$

The left hand side of (9) contains the same linear operators as the so called "telegraph equation", so the $\vec{E}$ field of (9) is unquestionably the causal radiation field generated by the sources on the right hand side of (9). The magnetic field, satisfying (2) and (3), is obtained from $\vec{E}$ by time integration of (3). Our discussion of sferic propagation will be based on (9).

Irrespective of the specific solutions of (9), some general properties of the solutions can be gleaned from an examination of the terms in the equation. The first two terms on the left hand side of (9) constitute the causal electromagnetic wave operator, while the third term represents the effect of finite-conductivity damping with a damping time

$$\tau = 1/\mu_o\sigma c^2 \qquad (10)$$

This damping time τ, a function of altitude, represents the maximal time scale of medium responses to impulsive sources. While a specific demonstration of this effect will be contrasted with observations in a later section, the typical dependence of τ and σ upon the altitude z is shown on Figure 9. From this figure, we observe that this maximal time scale decreases with altitude. Thus, if we imagine the propagation upwards of a complex signal structure, containing a spectrum of frequencies, the lower frequencies of the packet are allowed at low altitudes while only the higher frequency components can penetrate to higher altitudes. In a sinusoidal wave representation, this effect is often referred to as admittivity (Dejnakarintra and Park, 1974).

Next, the source terms on the right hand side of (9) need to be discussed. It is generally accepted that lightning discharge currents $\vec{J}_s$ generate sferics, but it must be noted also that the source term is not $\vec{J}_s$ but the time rate of change of $\vec{J}_s$; therefore, a correlative study of the sferic electric field signal structure with the discharge current structure must take this feature into account. Another interesting feature of (9) is that the gradient of charge distributions in the thundercloud is also a source of sferic radiation. Indeed, some sferic signals with polarity reversals appear to be strikingly similar in structure to polarity reversals of potential gradients in the thunderstorm cloud (Vonnegut et al., 1966). In any case, with two possible sferic sources to complicate matters, the presently available data do not permit an exhaustive study of the source structure; therefore, we shall attempt to discuss the propagation structure by considering the properties of Green's function solutions to the sferic equation (9).

Equation (9) is a linear scalar differential equation on a vector field with a vector source, which must be defined in terms of three independent scalar components functions although the three components are not coupled.

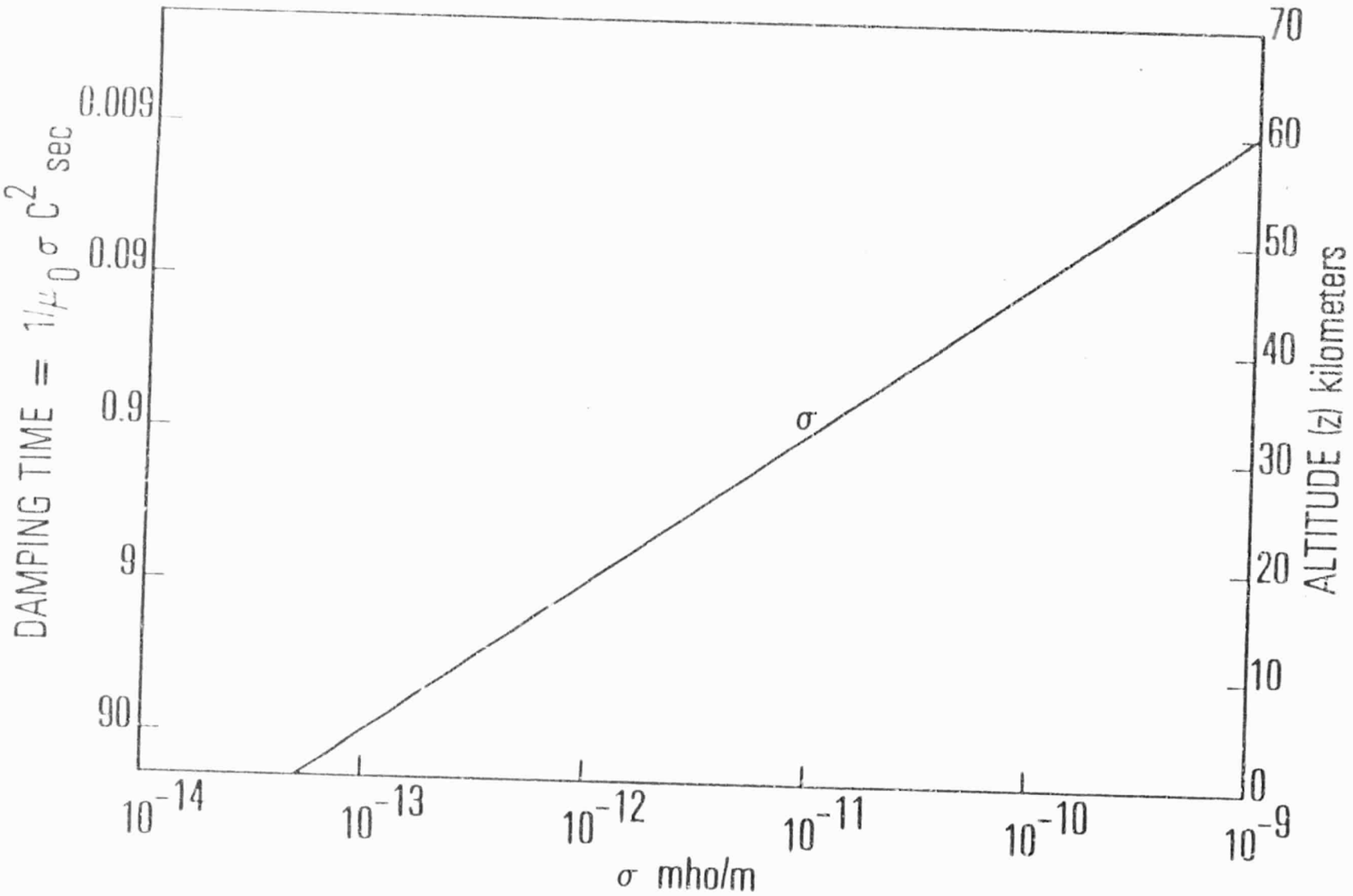

Figure 9. Conductivity and damping time plotted against altitude.

This important feature is especially important in the consideration of boundary conditions for $\vec{E}$. For example, in the limit of a perfectly conducting earth, the Green's function for the component E_ρ in a cylindrical coordinate system (ρ, z, ϕ) must satisfy the boundary condition $E_\rho = 0$ at the Earth's surface $z = 0$. Since the methods of constructing Green's functions satisfying such boundary conditions are standard [see for example Holzer and Saxon (1952) for the image source method, and Chiu and Hilton (1977) for integral equation methods], and since we are at present uncertain of the structure of the vector sources, we shall deal with the simplest elements of sferic propagation Green's function— that of infinite boundaries.

In view of the above discussion, it suffices for us to investigate the properties of the Green's function $G(\vec{r}, \vec{r}_o, t, t_o)$ for the scalar equation

$$\nabla^2 G - \frac{1}{c^2}\frac{\partial^2 G}{\partial t^2} - \mu_o \sigma(z) \frac{\partial G}{\partial t} = -4\pi \delta(\vec{r} - \vec{r}_o)\, \delta(t - t_o) \quad . \tag{11}$$

The conductivity $\sigma(z)$, with a typical altitude dependence shown on Figure 9, can be parameterized (below ~ 70 km) as

$$\sigma(z) = \sigma_o \exp(z/h) \tag{12}$$

where $\sigma_o = 5 \times 10^{-14}$ mho/m and $h = 6$ km. The Green's function G for (11) and (12) has not been considered although, as mentioned above, the sinusoidal wave solutions of (11) have been considered by many authors. We consider this problem in the limit of azimuthal symmetry (no ϕ dependence) in a cylindrical coordinate system (ρ, z, ϕ).

$$\frac{1}{\rho}\frac{\partial}{\partial\rho}\left(\rho\frac{\partial G}{\partial\rho}\right)+\frac{\partial^2 G}{\partial z^2}-\frac{1}{c^2}\frac{\partial^2 G}{\partial t^2}-\mu_o\sigma_o e^{z/h}\frac{\partial G}{\partial t}=-\frac{2}{\rho}\delta(\rho-\rho_o)\,\delta(z-z_o)\,\delta(t-t_o) \quad (13)$$

Using the delta function representations in sinusoidal and Bessel function form

$$\delta(t-t_o)=\frac{1}{2\pi}\int_{-\infty}^{\infty} e^{-i\omega(t-t_o)}\,d\omega \quad (14)$$

$$\frac{1}{x}\delta(x-x_o)=\int_o^{\infty} ydy\; J_\rho(xy)\; J_\rho(x_o y), \quad (15)$$

and transforming the coordinate z to a new coordinate $\xi \equiv \exp(z/2h)$ we can write an exact representation of G by the decompositional method [see for example Chiu and Hilton (1977)]:

$$G=\frac{2h}{\pi}\int_o^{\infty} kdk\int_o^{\infty}\lambda d\lambda\int_{-\infty}^{\infty} d\omega e^{-i\omega(t-t_o)}\,J_o(k\rho)J_o(k\rho_o)J_p(\lambda\xi)J_p(\lambda\xi_o)/$$

$$(\lambda^2-i4\mu_o\sigma_o h^2\omega) \quad (16)$$

where $p^2=4h^2(k^2-\omega^2/c^2)$. Because (16) involves integration over the order of Bessel functions, it is not tractable for the purposes of data interpretation even though the λ-integration of (16) can be carried out exactly by contour methods [see Watson (1966) p. 429].

The salient properties of (11) and (13) may however be discussed by other methods involving Green's function solutions. One such method is to consider a simplified but tractable version of (11) and (13) while keeping in mind that the simplification must not affect the essential properties of the solution. Such methods of considering a "surrogate" have been applied in many areas [see for example Chiu (1976)]. In the case of (13), we note that the character of

the equation involves causal propagation of a wave signal as well as "diffusion" damping from the linear time derivative term, which is the source of solution difficulties. To obtain a "surrogate" we note that if the conductivity is constant the causal propagation of the sferic wave is unaffected but we may gain insight to the sferic signal structure by eliminating mathematical difficulties.

If we assume the conductivity to be constant, an exact solution to (11) and (13) can be written in closed form (Morse and Feshbach, 1953, p. 868)

$$G = \frac{c}{2\pi R} e^{(-1/2)\,\mu_o \sigma c^2 (t-t_o)} \{\delta [c(t-t_o) - R] +$$

$$+ \frac{\mu_o \sigma c R}{2\sqrt{R^2 - c^2(t-t_o)^2}} J_1 [(1/2)\,\mu_o \sigma c \sqrt{R^2 - c^2(t-t_o)^2}]\, \theta [c(t-t_o)-R]\} \quad (17)$$

where $R^2 \equiv (\rho-\rho_o)^2 + (z-z_o)^2$, and $\theta(x) = 1$ if $x > 1$ and zero otherwise.

The character of the Green's function (17) becomes apparent if we consider the physical basis of each of the terms. The term $\delta [c(t-t_o)-R]/R$ is simply the Lienard-Wiechert potential of the causal electromagnetic radiation field. This is expected if sferics, at whatever frequency, are radiated signals. The finite conductivity of the medium $\sigma \neq 0$ gives rise to two effects. First, the entire signal structure is damped in time by the factor exp $[-(1/2)\mu_o \sigma c^2 (t-t_o)]$. Thus, $\tau \equiv 1/\mu_o \sigma c^2$ sets the upper limit to the time scale inspite of the source time scale implied in the Lienard-Weichert term. This effect is expected whether τ is constant or not, and it has been discussed previously in this section. In addition, the "diffusive" effect of the conduction current introduces a second, tail-like element in the signal structure in the form of the Bessel function term of (17). It should be noted that this effect is a tail-like signal because the causal condition (signified by

the θ-function) requires imaginary arguments for the Bes el function. The time scale of this tail is not exactly τ but is of the same order (~ a few seconds in the stratosphere), as we shall numerically illustrate in a later section. This tail-like structure may be a very important feature in data interpretation because, in contrast to media wave responses to impulsive disturbances, the sferic response in the stratosphere consists of a radiation pulse plus a single tail. This structure is borne out by observations in the preceeding section and discussed in more detail in the next section.

Next, let us investigate another "surrogate" of (13) which emphasizes the vertical structure, as imposed by $\sigma = \sigma_o \exp(z/h)$, but deemphasizes the causal element of the signal structure. In (17), the causal functions, $\delta[c(t-t_o) - R]$ and $\theta[c(t-t_o) - R]$, are formally very important, but for practical interpretation of signals received ≈ 100 km from the source the causal time delay is only of order of milliseconds or less. Therefore, for an instrument with response time longer than milliseconds it may be profitable to consider the implications of the vertical conductivity structure at the expense of maintaining causality. This means that we consider the Green's function in the "diffusion" limit of (13), i.e., $c \to \infty$ and the second time derivative term of (13) vanishes. In this limit, we obtain a Green's function representation

$$G = \frac{4h}{a^2}\,\theta(t-t_o)\int_o^\infty k\,dk\int_o^\infty p\,dp\; e^{-p^2(t-t_o)/a^2} J_{2hk}(p\xi)\, J_{2hk}(p\xi_o)\, J_o(kp)\, J_o(kp_o) \tag{18}$$

where $a^2 = 4\mu_o\sigma_o h^2$ and $\xi \equiv \exp(z/2h)$. The p-integration in (18) can be carried out with the identity

$$\int_o^\infty pdp\, e^{-p^2(t-t_o)/a^2} J_{2hk}(p\xi)\, J_{2hk}(p\xi_o) = \frac{a^2}{2(t-t_o)}\, e^{-\frac{a^2(\xi^2+\xi_o^2)}{4(t-t_o)}} \cdot$$

$$\cdot\, I_{2hk}\left[\frac{a^2\xi\xi_o}{2(t-t_o)}\right] . \qquad (19)$$

the Green's function (18) yields the classical "diffusive" elements of the form

$$G = \frac{2h\,\theta(t-t_o)}{t-t_o}\, e^{-\frac{a^2(\xi^2+\xi_o^2)}{4(t-t_o)}} \int_o^\infty kdk\, J_o(k\rho)\, J_o(k\rho_o)\, I_{2hk}\left[\frac{a^2\xi\xi_o}{2(t-t_o)}\right] . \qquad (20)$$

Note that $a^2\xi^2 \propto \sigma(z)$. In the stratosphere where $a^2 \approx 9 \times 10^{-12}$ sec^{-1} and $\xi \lesssim 10$, we note that the argument of I_{2hk} in (20) is very small for "tail-like" time scales $t-t_o \sim 10$ sec. Thus, for the "tail" part of the signal structure, we can use the approximation

$$I_{2hk}(x) = (x/2)^{2hk} = \exp\,[2hk\,\ln\,(x/2)] . \qquad (21)$$

Applying (21) to (20) and noting that the argument of I_{2hk} is less than unity, we obtain an approximate expression for the "tail" part of G by carrying out the integration in k in (20)

$$G = \frac{\theta\,(t-t_c)}{t-t_o}\, e^{-\frac{a^2(\xi^2+\xi_o^2)}{4(t-t_o)}} \frac{2\,\alpha\,h}{[\alpha^2 + (\rho-\rho_o)^2]^{3/2}} \qquad (22)$$

where

$$\alpha = 2h\,|\ln[a^2\xi\xi_o/4(t-t_o)]| \propto z \qquad (23)$$

Comparison of (22) to the "tail" part of (17) shows a number of revealing features despite the loss of the propagation parameter c in (22). First, the causal factor $\theta(t-t_o)/(t-t_o)$ in (22) directly corresponds to the causal factor $\theta[c(t-t_o) - R]/\sqrt{[R^2-c^2(t-t_o)]}$ in (17) in the limit $c \to \infty$. The damping factor in (22) has a time scale which is proportional to $1/\sigma(z)$ (because $a^2\xi^2 \propto \sigma(z)$) as in (17), although because of the loss of c in (22) the two time scales are very different. Nevertheless, we regard this feature as indication that the time scale $\tau \equiv 1/\mu_o\sigma c^2$ can be evaluated at various values of z even though (17) is derived with constant z. The scaling in the spatial structures of the signals in (17) and (22) are, however, very different. With the use of (23), we note that the spatial structure is roughly proportional to $z/[z^2 + (\rho-\rho_o)^2]^{3/2}$, as is usually expected in Green's functions of the operator ∇^2. The spatial structure of (17), for constant σ, is roughly 1/R. However, if one were to evaluate (17) with $\sigma=\sigma(z)$ then the magnitude of the "tail" structure will be dominated at high altitudes by the $\sigma(z)$ factor in the numerator. Considerations of (22) shows conclusively that this is unphysical. In other words, the evaluation of (17) with the artificial substitution $\sigma=\sigma(z)$ is roughly justified in determining time scales and horizontal spatial scales of the signal structure but is not justified in the interpretation of the magnitude of response as function of altitude. The altitude dependence $z/[z^2 + (\rho-\rho_o)^2]^{3/2}$ may be more truly representative of the signal structure.

In this section, we have attempted to review what has been done in the area of sferic signal propagation in the stratosphere. We have, in the process, carried the analysis one logical step further by considering the problem in terms of radiation and propagation in a conducting medium. The intimate interplay between the space-time structures of the source and of the propagation medium is shown to be interpretable in terms of Green's functions. While

it is rather unfortunate that an exact representation of the sferic Green's function requires numerical work far beyond what is appropriate for this book, investigation of some "surrogates" reveals properties which are borne out by balloon observations of sferic electric fields in the stratosphere.

V. DISCUSSION OF TIME CONSTANTS AND CURRENTS

In the last few sections we have presented a zoo of sferic observations in the stratosphere and the mathematical basis to help understand their propagation characteristics. Now we will use this theory and these observations in a few quantitative calculations in which we will attempt to explain some of the sferic signature characteristics and to calculate current densities associated with sferics.

The exact Green's function given in (17) has been approximated in (22) by assuming constant σ. Equation (22) was then evaluated at z=30 km using σ as given by equation (12). The upper plot in Figure 10 shows data from 0016 UT August 14, 1974 which included a small sferic that did not saturate our electronics (also see Figure 4). On top of the data is the plot of (22) after normalization of the amplitude to 3.54 volts at t=0. Since (22) assumes a constant σ (evaluated at z=30 km) it cannot be used to directly calculate the amplitude of the expected signal in the stratosphere as discussed in the last section. However (22) does give a good qualitative explanation of the sferic tail. The sferic tails seen in all of these data are shorter than the response time of the medium as shown in the bottom panel of Figure 10. This is a conductivity measurement on the same flight as the upper data taken about 3 hours later. In this measurement the upper vertical probe is internally shorted to payload ground for four seconds (t = -4 to 0 in Figure 10) and then refloated. The time response of the medium is inversely related to the ambient conductivity σ and in this case an exponential fit to the data after refloating gives a conductivity $\sigma = 6.2 \times 10^{-12}$ mho/meter with probe effects included. This incidentally compares very favorably to (12) which, when evaluated at z=30 km, gives σ(30 km) = 7.4×10^{-12} mho/m. For a more detailed

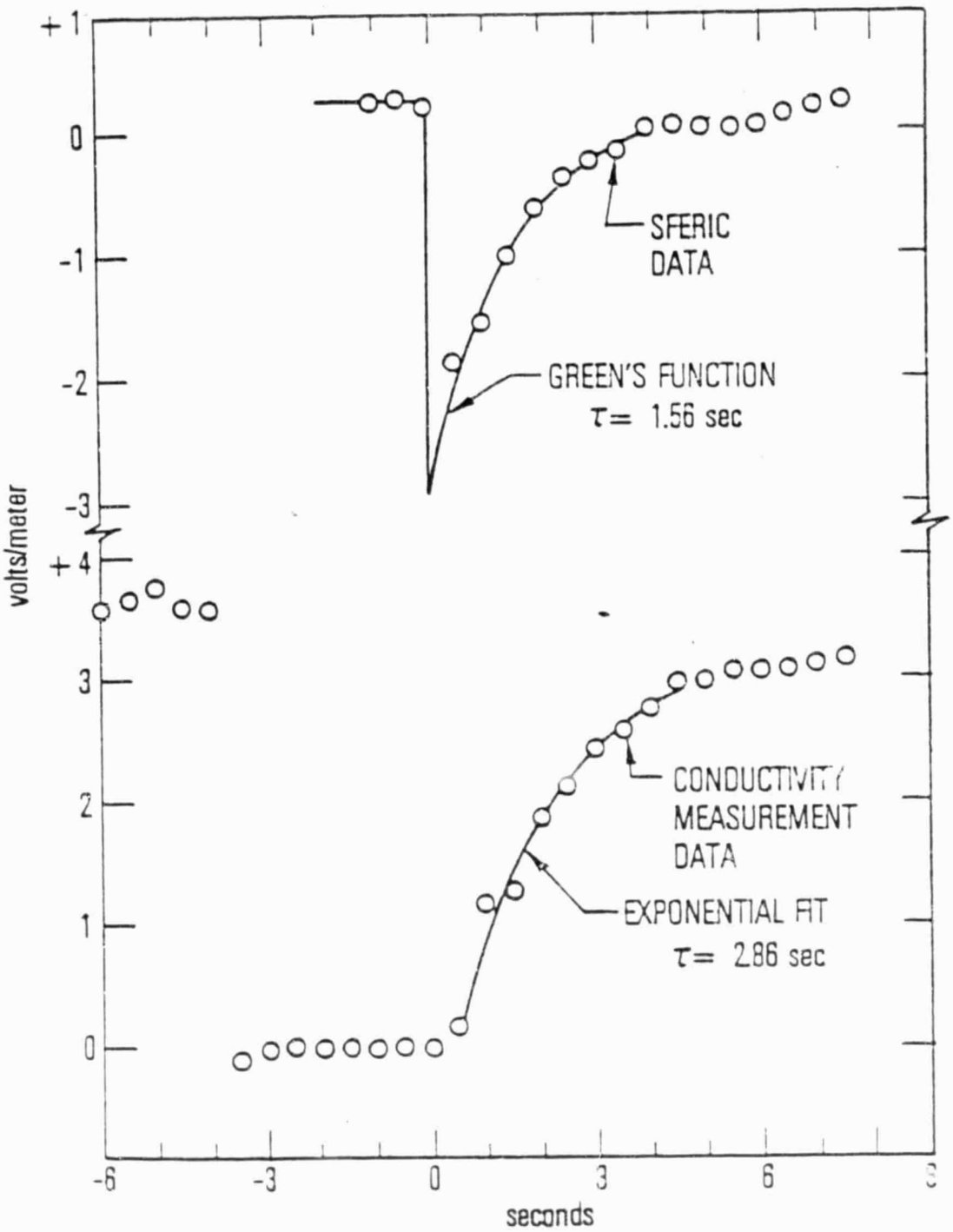

Figure 10. (Upper panel) About 10 seconds of raw electric field data -- surrounding the sferic observed at 0016.5 UT, August 14, 1974 (see also Figure 4). Plotted over the data in the upper panel is the Green's function from equation (22). The bottom panel is a conductivity measurement showing time response of the medium to be longer than the tail on the sferic by about a second. See text for more detail.

discussion of this type of conductivity measurement in the stratosphere see Holzworth (1980).

To emphasize the fact that the sferic tail really does decay faster than the ambient time response, the upper and lower data were both fit with exponentials resulting in time constants of τ = 1.56 seconds for the sferic (upper) and 2.86 sec for the conductivity measurements (lower). This shows that the sferic signal is indeed not simply an ohmic current but that the mathematical development in Section IV really is necessary to explain the propagation effects. It should also be noted that the final sferic return tails (from negative value near −4 volts track up to base line values of Figure 4 through 7 seen in the horizontal probes (lower panels with V_3 and V_4) are due to local time response effects after the ground fluctuation. The time constants determined from V_3 and V_4 following large sferics agree quite well with our probe shorting time responses.

The actual sferic current density flowing past the balloon cannot be unraveled easily from the electrical signature because of its nonohmic propagation effects. However, dramatic and complex ground fluctuations seen in all large sferics in Figures 4–7 and also by Bering (private communication, 1979) do result in redistribution of stratospheric ions and hence currents. In most cases the horizontal currents in the sferics are the same order of magnitude as the vertical.

The observed sferic signatures can be used, however, to place an upper limit on the current density and total current flowing in the stratosphere during a sferic. If the entire transient of the vertical field is assumed to drive an ohmic current it would have an average peak current density of $J_{avg} = \sigma E_{peak} = 6.2 \times 10^{-12}$ mho/m * 5 v/m = 31 pico amps/m. Thus 31 pico amps/m^2

is an upper limit to the peak sferic current density which might be much smaller. Comparing this upper limit to the actual dc current measured over a thunderstorm, which can be over 40 pico amps/m^2 for hours (see Figure 2 and Holzworth (1980)), the data show that sferics are probably not very important in charging up the ionosphere relative to the ground but that the dc dynamo currents driven by thunderstorm convection moves much more total charge than all the sferics together.

This chapter has provided an observational and theoretical background for the study of stratospheric sferic signals in the frequency range below 2 Hz. We have described the balloon borne high impedance electronic instruments used to detect the electric signals in this range and presented summary sferic data from dozens of balloon flights over and near thunderstorms. We then extended the theoretical background to treat radiation of sferic signals generated in the lower atmosphere with propagation into the stratosphere. This mathematical derivation of an electrical sferic equation resulted in an exact equation which was then simplified for sample calculations in order to help explain the temporal structure of the observed sferic signals. The observations in Section III can not be used as sferic source locations without a second balloon measurement so that the amplitude attenuation with distance can be calculated.

In this last section we applied the Green's function theory developed in Section IV in a sample calculation which helps to explain the time constants in the observed sferics. An upper estimate for the peak current density in a sferic was calculated assuming the observed sferic electric signature was all due to ohmic current. This is likely to be a gross overestimate but nevertheless shows that the total current carried to the ionosphere as a result of sferics is probably insignificant in comparison with the upward dc current over thunderstorms.

Much can be gained in a further study of sferics by higher time resolution instrumentation and multiple simultaneous observations. Also more accurate approximations to equation (17) would allow more useful comparison to the observed sferics. Sferic research in the stratosphere has just begun and this chapter attempts to tie some of this early work together.

Acknowledgments

The authors would like to thank F. Mozer and E. Bering for helpful discussions and D. Boucher for mathematical support.

Data used in this chapter were collected while R. Holzworth was at the University of California working under NSF grants GA33112X and ATM76-22278 and office of Naval Research contract N00014-75-C-0294. The analysis conducted for this chapter were supported in part by NASA contract NASW-3327 to The Aerospace Corporation.

REFERENCES

Anderson, F. J. and G. D. Freier, Interactions of the thunderstorm with a conducting atmosphere, J. Geophys. Res., 74, 5390, 1696.

Atkinson, W., S. Lundqvist, and U. Fahleson, The electric field existing at stratospheric elevations as determined by tropospheric and ionospheric boundary conditions, Pure Appl. Geophys., 84, 46, 1971.

Benbrook, J. R., J. W. Kern and W. R. Sheldon, Measured Electric Field in the Vicinity of a Thunderstorm System at an Altitude of 37 km, J. Geophys. Res., 79, 5289, 1974.

Bostrom, R., and U. Fahleson, Vertical propagation of time-dependent electric fields in the atmosphere and ionosphere, contributed paper Fifth International Conference on Atmospheric Electricity, Garmisch-Partenkirchen, 2-7 September, 1974.

Burke, H. -H.K., Large Scale Atmospheric Electric Fields: Comparisons with Balloon Data, Ph.D. Thesis Dept. of Space Physics and Astronomy, Rice University, Houston, pp. 128, 1975.

Chiu, Y. T., Self-consistent electrostatic field mapping in the high-latitude ionosphere, J. Geophys. Res., 79, 2790, 1974.

Chiu, Y. T., Planetary scale wave response to auroral heating of the neutral atmosphere, J. Geophys. Res., 81, 1231, 1976.

Chiu, Y. T., and H. H. Hilton, Exact Green's function method of solar force free magnetic field computations with constant , I. theory and basic test cases, Ap. J., 212, 873, 1977.

Dejnakarintra, M., and C. G. Park, Lightning-induced electric fields in the ionosphere, J. Geophys. Res., 79, 1903, 1974.

Holzer, R. E., and D. S. Saxon, Distribution of electrical conduction currents in the vicinity of thunderstorms, J. Geophys. Res., 57, 207, 1952.

Holzworth, R. H., High Latitude Stratospheric Electrical Measurements in Fair and Foul Weather under Various Solar Conditions, J. Atmos. Terr. Phys. in press, 1980.

Holzworth, R. H., J.-J. Berthelier, D. K. Cullers, U. V. Fahleson, C. -G. Falthammar, M. K. Hudson, L. Jalonen, M. C. Kelley, P. J. Kellogg, P. Tanskanner, M. Temerin and F. S. Mozer, The large scale ionospheric electric field: its variation with magnetic activity and relation to terrestrial kilometric radiation, J. Geophys. Res., 82, 2735, 1977.

Illingworth, A. J., Electric field recovery after lightning as the response of the conducting atmosphere to a field charge, Quart. J. Roy. Meteorol. Soc., 98, 604, 1972.

Kellogg, P. J., and M. Weed, in Planetary Electrodynamics, S. C. Coroniti and J. Hughes (ed.), Vol. 2, p. 431, Gordon and Breach, N. Y., 1969.

Morse, F. M., and H. Feshbach, Methods of Theoretical Physics, Vol. I, p. 868, McGraw-Hill, N.Y., 1953.

Mozer, F. S., Power spectra of the magnetospheric electric field, J. Geophys. Res., 76, 3651, 1971a.

Mozer, F. S., Balloon measurement of vertical and horizontal atmospheric electric fields, Pure Appl. Geophys., 84, 32, 1971b.

Mozer, F. S. Analyses of techniques for measuring DC and AC electric fields in the magnetosphere, Space Sci. Rev., 14, 272, 1973.

Mozer, F. S. and P. Lucht, The average auroral zone electric field, J. Geophys. Res., 79, 1001, 1974.

Mozer, F. S. and R. Serlin, Magnetospheric electric field measurements with balloons, J. Geophys. Res., 74, 4739, 1969.

Park, C. G., and M. Deinakaritra, Penetration of thundercloud electric fields into the ionosphere and magnetosphere, 1., Middle and sub-auroral latitudes, J. Geophys. Res., 78, 6623, 1973.

Reid, G. C., Ionospheric effects of electrostatic fields generated in the outer magnetosphere, Radio Sci., 69D, 827, 1965.

Stergis, C. G., G. C. Rein and T. Kangas, Electric field measurements above thunderstorms., J. Atmos. Terr. Phys., 11, 83, 1957.

Volland, H., Mapping of the electric field of the Sq current into the lower atmosphere, J. Geophys. Res., 77, 1961, 1972.

Vonnegut, B., C. B. Moore, R. P. Espinola, and H. H. Blau, Jr., Electric potential gradients above thunderstorms, J. Atmos. Sci., 23, 764, 1966.

Wait, G. R., Aircraft measurements of electric charge carried to ground through thunderstorms, in Thunderstorm Electricity, pp. 191-206, Univ. of Chicago Press, Chicago, 1953.

Watson, G. N., A Treatise on the Theory of Bessel Functions, p. 429, Cambridge University Press, London, 1966.

Exhibit D: Correlative Study of Thermospheric Gravity Waves and Tropospheric Vorticity Area Index, by Y. T. Chiu and L. R. Sharp

Correlative Study of Thermospheric Gravity Waves and Tropospheric Vorticity Area Index

Y. T. Chiu and L. R. Sharp
Space Sciences Laboratory
The Aerospace Corporation
El Segundo, California 90245

September 1980

Submitted to Geophysical Research Letters

This work is supported in part by NASA Grant NASW-3327
and by The Aerospace Supported Research Program

Abstract

Based on the occurrence frequency of wave-like structures in some 24,000 measurements of thermospheric density, we demonstrate that there is no significant hemispherical correlation between satellite-measured thermospheric wave-like structures and the tropospheric vorticity area index in the epoch 1974-1976. However, in the northern polar zone, (60°-90°) N, wave occurrence frequency is greater for large values of the 500 mb vorticity area index.

INTRODUCTION

In two previous studies of the geographical distributions of wave-like density disturbances in the thermosphere, it was established that the distributions show patterns of occurrence which match persistent features of the troposphere, such as regions of strong wind shear associated with the subtropical jet stream (Rice and Sharp, 1977) and seasonably persistent regions of deep convective activity indicated by high occurrence rates of lightning at dawn (Chiu et al., 1979). Such studies, together with studies of the auroral origin of large-scale thermospheric wave-like density disturbances (Potter et al., 1976), offer suggestions as to the origin of persistent global-scale sources of thermospheric gravity waves, which we identify a priori with the thermospheric wave-like density disturbances discussed in the above studies. At the small-scale end of the spectrum of atmospheric disturbances, thermospheric waves associated with local-scale (mesoscale) disturbances of the troposphere, such as thunderstorms, tornadoes and hurricanes, have also been reported (Hung et al., 1978). Thus, considering the entire spectrum of atmospheric disturbance scales as a whole, one is naturally prompted to ask if a similar correlation between satellite-measured thermospheric disturbances and transient synoptic scale (weather) systems in the troposphere may not also exist.

The existence or non-existence of such a correlation has significant implications for the viability of some suggested physical mechanisms for the so-called "sun-weather" effect (cf. Wilcox et al., 1976); in particular, those mechanisms requiring transmission or modification of an atmospheric disturbance between the upper and lower atmosphere will be affected. For example, Hines and Halevy (1975) suggested that a "solar influence must somehow modu-

late the meteorological noise" to produce the "sun-weather" signal. A condition for such physical mechanisms to be viable is that there exists a relationship between "meteorological noise" of the proper scale in the upper and lower atmospheres. In this correlative study of upper and lower atmospheric data of "meteorological noise," we do not address the question of the "sun-weather" effect; rather, we focus upon the correlation, if any, of satellite-measured upper atmospheric "meteorological noise" with that of the troposphere as is indicated by the vorticity area index (VAI). Although we demonstrate that there is no significant hemispherical correlation between satellite-measured thermospheric wave-like structures and the tropospheric vorticity area index in the epoch 1974-1976, we cannot make any comments on the "sun-weather" effect in general because it is possible that the solar signal can be carried by upper atmospheric "noise" in portions of the scale spectrum not covered by our satellite data. In the high-latitude region (60°-90°) N, thermospheric wave occurrence does depend upon the vorticity area index. If this correlation is to be identified with the "sun-weather" effect, then the likely mechanism would be thermospheric processes associated with polar phenomenon such as the aurora.

DATA AND ANALYSIS

The correlation study involves two sets of data. The lower atmospheric data set is the vorticity area index (VAI) for 1974-1976 compiled by R. G. Olson, W. O. Roberts and E. Gerety (Shapley and Kroehl, 1977). The VAI values, in units of 10^5 km^2, are derived from the 500 mb height analysis records of the U. S. National Meteorology Center for the northern hemisphere above 10° N, and for both 0000 UT and 1200 UT. The upper atmospheric data set consists of 24,000 density measurements in the northern hemisphere some of which contain wave-like structures. These data were obtained from cold cathode ion gauges onboard Atmospheric Explorer spacecrafts AE-C, AE-D, AE-E and the Air Force spacecraft S3-1. Data obtained in the altitude range 135-225 km are used. A description of the cold cathode ion gauge is given in Rice et al. (1973). Figure 1 of Reference A (Chiu et al., 1979) depicts a relatively disturbed neutral density profile as a function of altitude; similar wave-like structures observed by other instruments onboard AE-C have been interpreted as gravity waves (Reber et al., 1975). In this figure, four classes of wave-like structures are illustrated; the four wave classifications are identified with an index value running from 1 to 4 (Rice and Sharp, 1977). The classifications are: I = 1, indicating a smoothly varying profile; I = 2, indicating minor activity with up to 5% density amplitude, I = 3, indicating waves of 5-15% density amplitude peak to peak; and I = 4, indicating waves of density amplitude greater than 15%. For this study, wave classifications 3 and 4 have been combined as an indication of the unambiguous presence of a gravity wave. Although in general wave classifications 3 and 4 have different wavelengths, we have not yet found any indication that they originate from different sources. For the data from AE-D, we have excluded

periods when the spacecraft was undergoing nutation. In addition to data used in Reference A, data from the AE-E satellite have been added to the data base, comprising a total of 23,691 density measurements at 5 km altitude intervals of the above satellites in the northern hemisphere in the period 1974-1976.

The thermospheric index is the wave occurrence frequency (WOF) which is defined as the percentage of wave measurements of classes 3 and 4 found in the portion of the total number of measurements (23,691) which corresponds to the stated conditions of the particular correlation parameter. Thus, if a certain WOF is 0.24 for a stated correlation condition, then classes 3 and 4 waves are found in 24% of the density measurements corresponding to that condition. Generally, if a relationship exists, the WOF will depend on the VAI; and this relationship is quantified in a plot of WOF as function of VAI. The error analysis for this relationship is particularly simple if we assume normal distributions. If waves are found in N samples of a total of M appropriate measurements, the WOF is $(N/M) \pm (\sqrt{N}/M)$. The results of the correlations are stated in WOF because satellite measurements are not evenly distributed in space and time and VAI mean values also vary secularly in the period 1974-1976.

1. Hemispherical relationship between WOF and VAI. Figure 1 shows the relationship between WOF and VAI for the northern hemisphere for three time shifts between the indices. The numbers near the bottom of the figure indicate the distribution of measurements in each VAI interval for 0 day time shift (measurement distributions for other time shifts are similar). Evidently, VAI values in the sampling period do not form a normal distribution. Nevertheless, the significant result of this figure is that thermospheric wave occurrence frequency (WOF) in the northern hemisphere is $\approx (25 \pm 5)\%$, independent of VAI values. Even though the 5% fluctuations shown are outside of

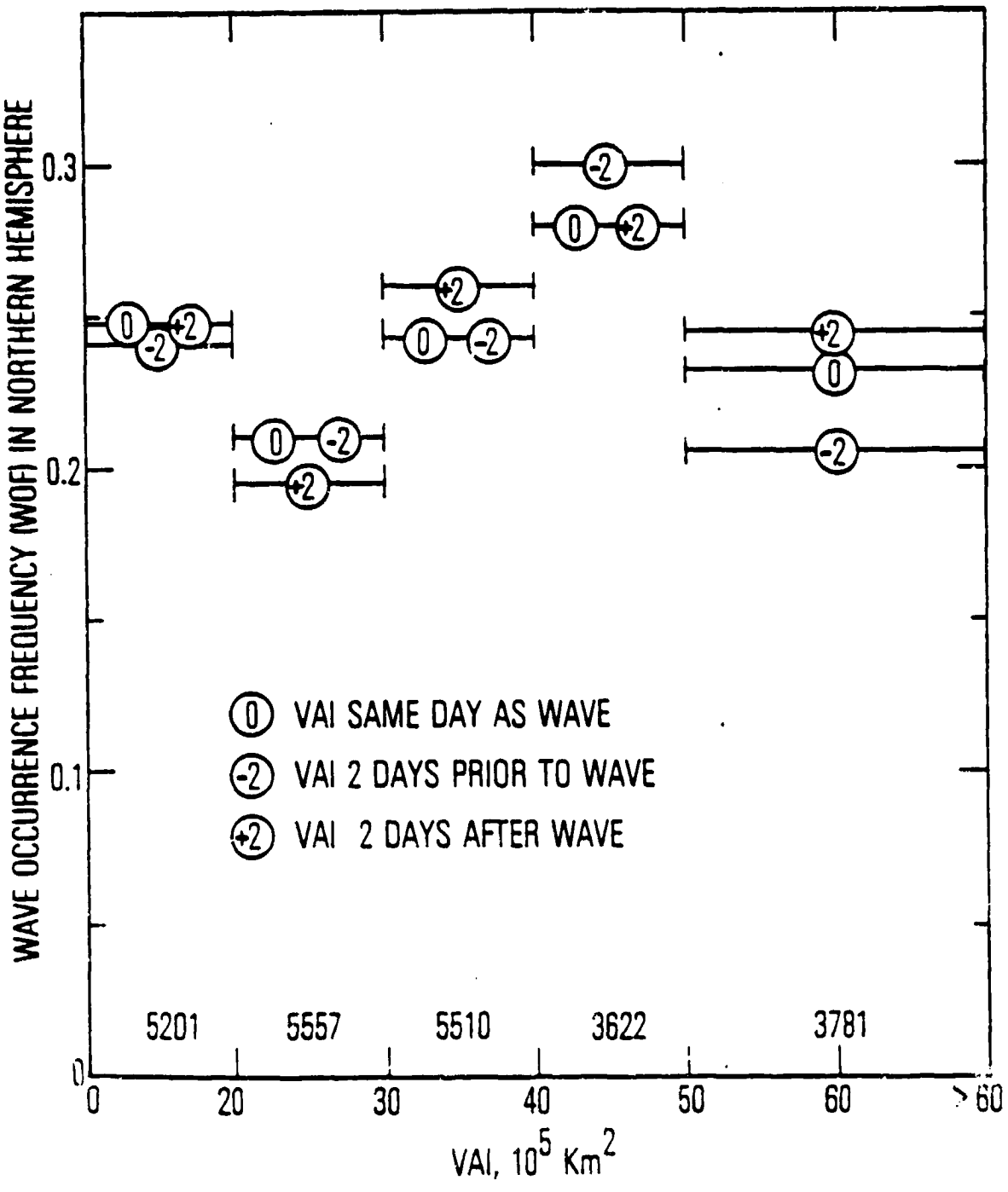

Figure 1. Correlation between wave occurrence frequency in the northern hemisphere and the vorticity area index.

normally distributed statistical limits, possible dependence of the WOF upon the VAI at the < 5% level is hardly of significance.

2. Zonal relationship between WOF and hemispherical VAI. Figure 2 shows the relationship between WOF in the polar (60°N-90°N, P), mid-latitude (30°N-60°N, M) and equatorial (0°N-30°N, E) zones and the hemispherical VAI at 0 day time shift. Except for statistical fluctuation in the (40-50) x 10^5 km^2 bin of VAI, the WOF in the equatorial (E) and mid-latitude (M) zones (and/or the sum of the two) is again independent of VAI, at a value of ≈ (22 ± 5)%. The WOF for the polar (P) zone shows a significant (factor of two) jump from ~ 15% to ~ 30% for VAI values greater than 30 x 10^5 km^2. Similar dependence is found for ± 2 day time shifts. Examination of the measurement distributions among the three zones (bottom of Figure 2) indicates that the centroid of VAI for the polar zone (~ 50 x 10^5 km^2) is higher than that of the other two zones (~ 25 x 10^5 km^2). This prompts us to note that most polar zone data come from the polar-orbiting AE-D in the epoch (Nov. 1974 - Jan. 1975) when VAI values happened to be high because of the northern winter. Thus, the strong dependence of the polar zone WOF upon the VAI may be due to preferential sampling of wintertime VAI by the AE-D satellite at high latitudes; nevertheless, it cannot be denied that WOF is also unusually high during this interval irrespective of sampling.

Because of the abnormal measurement distribution, we examine this "latitude" effect further by contrasting the AE-D data with the AE-C data, which also contribute to the polar zone. The AE-C data extends up to only 68° N. Figure 3 shows the polar zone WOF for the AE-C and AE-D data as functions of VAI at zero time shift. The centroid of the measurement distribution for the AE-C data set is at VAI ≈ 35 x 10^5 km^2 while that for the AE-D data set is at VAI ≈ 50 x 10^5 km^2. Both data sets show a substantial increase in the polar

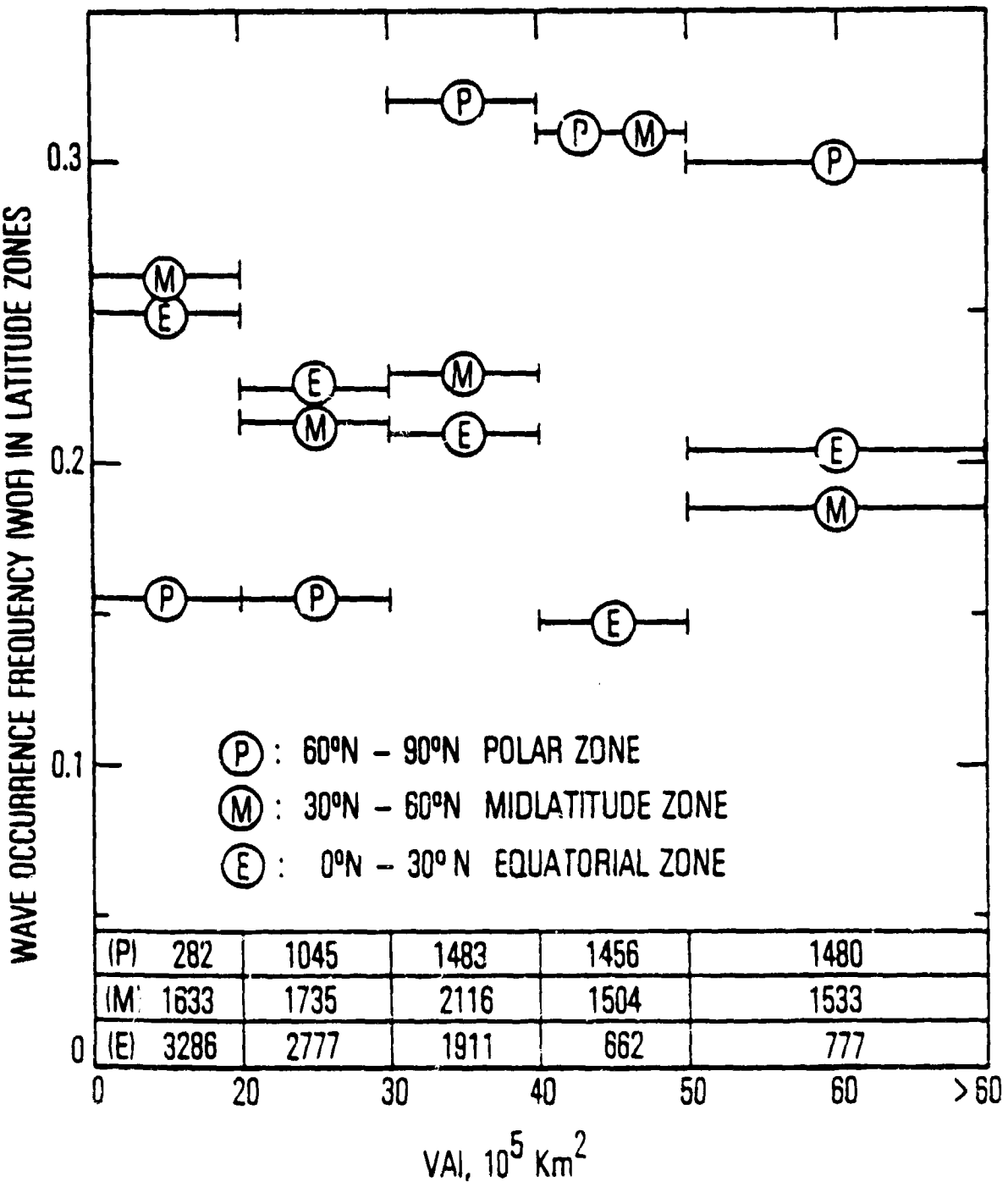

Figure 2. Correlation between wave occurrence frequency in the equatorial, mid-latitude and polar zones with the vorticity area index.

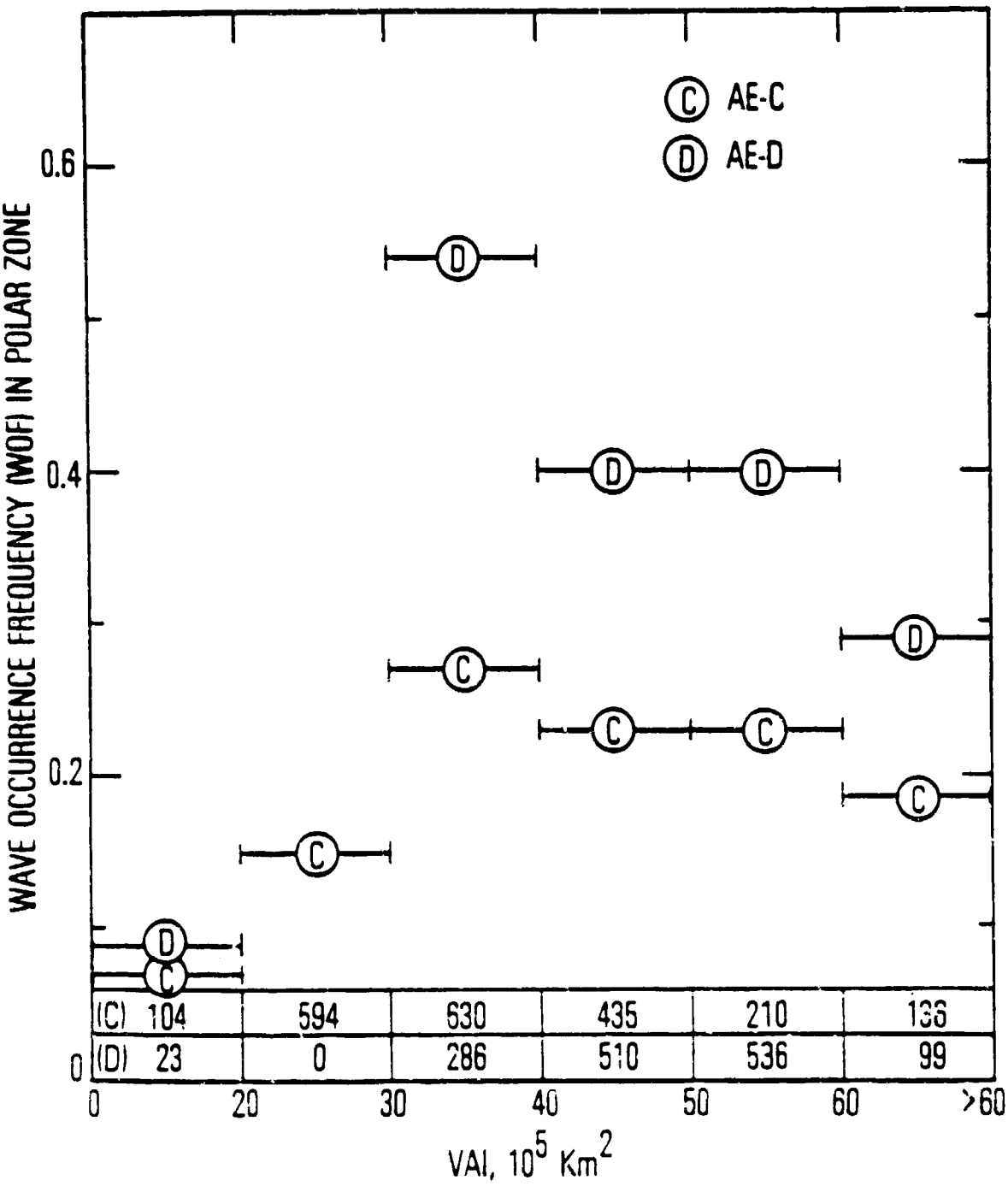

Figure 3. Correlation between wave occurrence frequency in the polar zone with the vorticity area index for the AE-C and AE-D data sets.

zone WOF as VAI increases past 30 x 10^5 km^2. Therefore, it is likely that the polar zonal relationship between WOF and hemispherical VAI shown on Figure 2 is really a latitude effect and not due to sampling bias of the AE-D satellite. Even if we discount Figure 3, we emphasize that the polar zone data clearly shows dependence of WOF upon the VAI, although one would not then be able to say whether it is due to a latitude effect alone or due to a secular increase of the average VAI during the AE-D sampling period.

If this polar zone effect has some relationship with the "sun-weather" effect, then it would argue for upper-lower atmospheric wave coupling associated with polar phenomena such as auroral processes. We offer this as a speculative comment since the "sun-weather" effect need not be germane to our specific discussion of upper and lower atmospheric wave correlations.

3. Hemispherical relationships between WOF, VAI and interplanetary magnetic sector boundary crossings. In Figure 4, we show the northern hemisphere WOF and VAI, averaged over the measurement distribution (shown at the bottom of the figure), within ± 6 days of interplanetary magnetic sector boundary crossings in epoch 1974-1976. Even though the average VAI is taken over an uneven measurement distribution, the characteristic signature of VAI dependence on days from sector boundary (Wilcox et al., 1976) is found. The hemispherical WOF, however, remains at ~ (25 ± 5)%, independent of days from sector boundary crossings. We have also examined the relationship between polar zone WOF and the interplanetary magnetic sector boundary crossings. Again, we found that the polar zone WOF to be independent of days from sector boundary crossings, although we have only a small data set to work with.

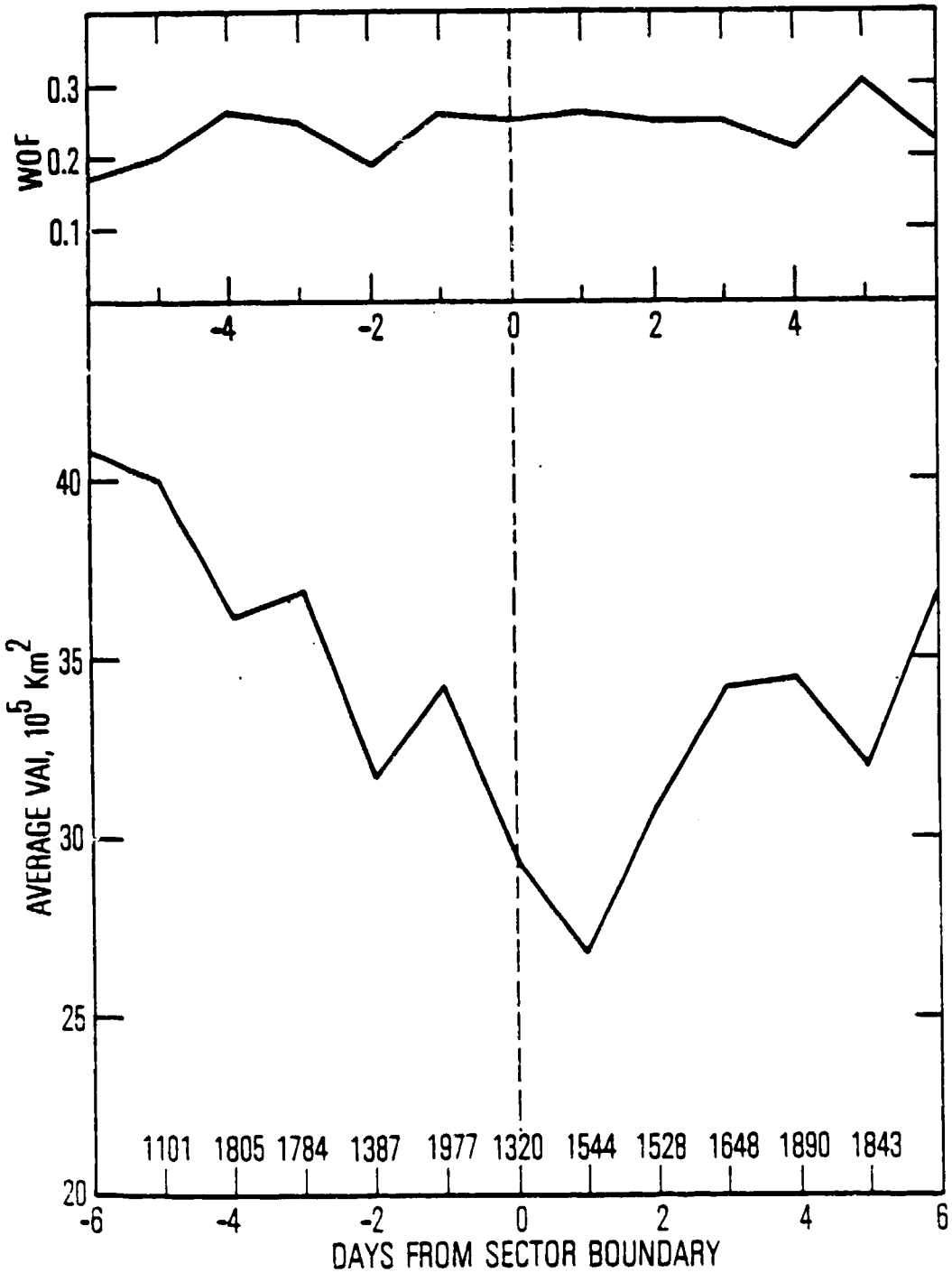

Figure 4. Average vorticity area index and hemispherical wave occurrence frequency in relation to interplanetary magnetic sector boundary crossings.

CONCLUSIONS

Based on the occurrence frequency of thermospheric wave structures in some 24,000 measurements of density, we demonstrate that there is no significant hemispherical correlation between thermospheric waves and the tropospheric vorticity area index in the epoch 1974-1976. Further, wave occurrence frequency does not exhibit the characteristic feature of the VAI in relation to interplanetary magnetic sector boundary crossings. In the polar zone, (60° - 90°) N, wave occurrence frequency does increase significantly if the hemispherical VAI increases above ~ 30 x 10^5 km^2. In contrast to previous work (Rice and Sharp, 1977; Chiu et al., 1979), which correlated thermospheric wave occurrence to geographically and seasonally persistent features of the troposphere, this work focuses upon the study of transient (weather) systems as represented by the VAI. Consequenly, the null relationship between VAI and the wave occurrence frequency outside the polar zone may reflect the dominance of the persistent sources in the non-polar troposphere.

ACKNOWLEDGMENT

This work is supported in part by NASA Grant NASW-3327 and by the Aerospace Supported Research Program.

References

Chiu, Y. T., B. C. Edgar, C. J. Rice and L. R. Sharp, A correlation of thermospheric gravity waves with tropospheric lightning, Geophys. Res. Lett. 6, 45, 1979.

Hines, C. O. and I. Halevy, Reality and nature of a sun-weather correlation, Nature 258, 313, 1975.

Hung, R. J., T. Phan and R. E. Smith, Observation of gravity waves during the extreme tornado outbreak of 3 April 1974, J. Atmos. Terr. Phys. 40, 831, 1978.

Potter, W. E., D. C. Kayser and K. Mauersberger, Direct measurement of neutral wave characteristics in the thermosphere, J. Geophys. Res. 81, 5002, 1976.

Reber, C. A., A. E. Hedin, D. T. Pelz, W. E. Potter and L. H. Brace, Phase and amplitude relationships of wave structure observed in the lower thermosphere, J. Geophys. Res. 80, 4576, 1975.

Rice, C. J. and L. R. Sharp, Neutral atmospheric waves in the thermosphere and tropospheric weather systems, Geophys. Res. Lett. 4, 315, 1977.

Rice, C. J., V. L. Carter, S. R. LaValle, W. T. Chater, D. A. Jones, C. G. King and D. F. Nelson, Atmosphere explorer pressure measurements: Ion gauge and capacitance manometer, Radio Sci. 8, 305, 1973.

Shapley, A. J. and H. W. Kroehl, Solar-terrestrial physics and meteorology, working document II, SCOSTEP/U. S. National Academy of Sciences, Washington, D.C., 1977.

Wilcox, J. M., L. Svalgaard and P. H. Scherrer, On the reality of a sun-weather effect, J. Atm. Sci. 33, 1113, 1976.